Mitochondrial ETF insufficiency drives neoplastic growth by selectively optimizing cancer bioenergetics

David Papadopoli[1,2], Ranveer Palia[1,3], Predrag Jovanovic[1,3], Sébastien Tabariès[4], Emma Ciccolini[1,3], Valerie Sabourin[1], Sebastian Igelmann[5], Shannon McLaughlan[6], Lesley Zhan[6], HaEun Kim[3], Nabila Chekkal[6], Krzysztof J. Szkop[7], Thierry Bertomeu[8], Jibin Zeng[1], Julia Vassalakis[9], Farzaneh Afzali[9], Slim Mzoughi[10], Ernesto Guccione[10], Mike Tyers[11], Daina Avizonis[4,12], Ola Larsson[7], Lynne-Marie Postovit[9], Sergej Djuranovic[13], Josie Ursini-Siegel[1,2,3,6], Peter M. Siegel[3,4,6], Michael Pollak[1,2,3*], Ivan Topisirovic[6*]

[1]Lady Davis Institute, SMBD JGH, McGill University, Montréal, QC H3T 1E2, Canada.

[2]Gerald Bronfman Department of Oncology, McGill University, Montréal, QC H3A 0G4, Canada.

[3]Department of Experimental Medicine, McGill University, Montréal, QC H3A 0G4, Canada.

[4]Rosalind and Morris Goodman Cancer Institute, McGill University, Montréal, QC H3A 1A3, Canada

[5]VIB Center for Cancer Biology, Department of Oncology, KU Leuven and Leuven Cancer Institute (LKI), Herestraat 49, 3000 Leuven, Belgium.

[6]Department of Biochemistry, McGill University, Montréal, QC H3A 0G4, Canada.

[7]Department of Oncology-Pathology, Science for Life Laboratory, Karolinska Institute, 171 77, Stockholm, Sweden.

[8]Institute for Research in Immunology and Cancer, Université de Montréal, Montréal, QC H3T 1J4, Canada.

[9]Department of Biomedical and Molecular Sciences, Queen's University, Kingston, ON K7L 3N6, Canada.

[10]Center of OncoGenomics and Innovative Therapeutics (COGIT), Department of Oncological Sciences, Tisch Cancer Institute, Icahn School of Medicine at Mount Sinai, New York, NY, 10029 United States

[11]Program in Molecular Medicine, The Hospital for Sick Children, Toronto, ON M5G 0A4, Canada. Department of Molecular Genetics, University of Toronto, Toronto, ON M5S 1A8, Canada.

[12]Metabolomics Innovation Resource, McGill University, Montréal, QC, Canada.

[13]Department of Cell Biology and Physiology, Washington University School of Medicine, St. Louis, MO 63110, United States

[*]Correspondence michael.pollak@mcgill.ca (M.P.), ivan.topisirovic@mcgill.ca (I.T.)

Keywords: Electron transfer flavoprotein dehydrogenase (ETFDH), cancer metabolism, mRNA translation, mechanistic target of rapamycin (mTOR), 4E-binding protein 1 (4E-BP1).

Abstract

Mitochondrial electron transport flavoprotein (ETF) insufficiency causes metabolic diseases known as a multiple acyl-CoA dehydrogenase deficiency (MADD). Although essential in muscle, we identified ETF dehydrogenase (ETFDH) as one of the most dispensable metabolic genes in neoplasia, and its expression is reduced across human cancers. ETF insufficiency caused by decreased ETFDH expression limits flexibility of OXPHOS fuel utilization but paradoxically increases cancer cell bioenergetics and accelerates neoplastic growth by retrograde activation of the mTORC1/BCL-6/4E-BP1 axis. Collectively, these findings reveal that while ETF insufficiency is rare and has detrimental effects in non-malignant tissues, it is common in neoplasia, where ETFDH downregulation leads to bioenergetic and signaling reprogramming that accelerate neoplastic growth.

Main

The mitochondrial electron transport chain (ETC) transfers electrons from reducing equivalents (NADH and $FADH_2$) towards complexes I/II, or from peripheral metabolic enzymes that reduce coenzyme Q (ubiquinone, Q) to ubiquinol (QH_2) [1]. The electron transfer flavoproteins (ETFA and ETFB) accept electrons generated by the catabolism of branched-chain amino acids and fatty acids [2-4]. ETFs interact with ETF dehydrogenase (ETFDH or ETF-ubiquinone oxidoreductase) [5], which controls electron flow towards complex III (Supplementary Fig.1A). Loss-of-function mutations in ETF/ETFDH occur in metabolic diseases known as multiple acyl-CoA dehydrogenase deficiency (MADD) [6,7]. ETFDH is also essential for complex III activity in skeletal muscle [8]. Surprisingly, we observed that in contrast to muscle, ETFDH is one of the most non-essential metabolic genes in cancer cells. Paradoxically, ETFDH downregulation leads to enhanced mitochondrial biogenesis and increased bioenergetic capacity of cancer cells. ETF insufficiency resulting from reduction in ETFDH levels triggers a tradeoff favored by cancer cells, whereby reduced flexibility in fuel utilization for oxidative phosphorylation is offset by retrograde signaling that remodels cancer cell bioenergetics to augment neoplastic growth.

ETFDH is dispensable in cancer cells and its abrogation accelerates tumor growth

ETFDH is essential in skeletal muscle cells [8]. Intriguingly, a CRISPR-Cas9 knock out (KO) screen performed in a human acute lymphoblastic leukemia cell line (NALM6) [9] ranked *ETFDH* as a top non-essential metabolic gene that clustered with well-established tumor suppressors *TP53* and *RB1* (Supplementary Fig.1B). Mining DepMap also revealed that *ETFDH* is essential in only 1 out of 1150 cancer cell lines [10]. This motivated us to examine the role of ETFDH in cancer. *ETFDH* mRNA levels are reduced in patient samples across different cancer types, including colon

(Supplementary Fig.1C) and breast cancer (Supplementary Fig.1D). Immunohistochemistry (IHC) staining confirmed that ETFDH protein levels are significantly reduced in colorectal cancer vs. non-adjacent patient-derived tissues (NAT) (Fig.1A).

We next abrogated the *ETFDH* gene using a CRISPR-Cas9 approach in a variety of cancer cell lines including HCT-116 (human colorectal cancer), NT2197 (murine HER2+ breast cancer), 4T1 (murine triple negative breast cancer cells), and NALM6 cells (Supplementary Fig.1E-H). We also investigated the effects of ETFDH loss in non-transformed normal murine mammary gland (NMuMG) cells (Supplementary Fig.1I), a parental immortalized mammary epithelial cell line that was transformed with an oncogenic ErbB2 variant to generate NT2197 cells [11]. Notwithstanding their high baseline proliferation rates, ETFDH ablation significantly increased proliferation across all tested cancer cell lines (Supplementary Fig.1E-H). This was not caused by the inadvertent effects of the CRISPR-Cas9, as rescuing ETFDH expression in HCT-116 and NT2197 cells reverted proliferation rates to levels comparable to ETFDH-proficient controls (Supplementary Fig.1E-F). In contrast, ETFDH abrogation did not affect proliferation of non-transformed NMuMG cells (Supplementary Fig.1I). ETFDH KO HCT-116 cells also formed more colonies in soft agar (surrogate measurement of cellular neoplastic potential [12]) as compared to empty vector infected controls (WT EV), and ETFDH KO cells in which ETFDH was re-expressed (ETFDH Rescue) (Supplementary Fig.1J).

Based on these findings, we tested the impact of ETFDH loss on neoplastic growth *in vivo.* WT EV, ETFDH KO, or ETFDH Rescue HCT-116 cells were injected orthotopically in the caeca of SCID-BEIGE mice. Loss of ETFDH significantly increased the tumor growth rate and volume at endpoint relative to control and ETFDH Rescue cells (Fig.1B-C). ETFDH loss also increased NT2197 tumor growth and the final tumor volume as compared to ETFDH-proficient tumors

following orthotopic mammary fat pad injections in SCID-BEIGE mice (Fig.1D-E). Altogether, these results show that *ETFDH* is an non-essential gene in cancer that is under-expressed across different cancer types, and that its disruption enhances neoplastic growth, while not affecting proliferation of non-transformed cells.

ETFDH abrogation results in ETF insufficiency that paradoxically increases bioenergetic capacity of cancer cells

In non-cancerous cells, ETFDH transfers electrons from catabolism of fatty acids and amino acids to the ETC (Supplementary Fig.2A). Palmitate oxidation (monitored by oxygen consumption) and ^{13}C leucine labelling into citrate (citrate m+2) were strongly attenuated by ETFDH abrogation in HCT-116 cells (Supplementary Fig.2B-C), which confirmed that ETF plays a role in fatty and amino acid catabolism in malignant cells. Thus, ETFDH loss induces ETF insufficiency in cancer cells that mirrors defects observed in non-malignant tissues. Surprisingly, ETFDH loss in HCT-116 cells increased oxygen consumption and extracellular acidification, relative to control WT EV and ETFDH Rescues (Fig.2A-B). ETFDH KO HCT-116 cells produced higher levels of ATP from oxidative phosphorylation (*J* ATP ox) as compared to ETFDH-proficient cells (Fig.2C-D). Consequently, ETFDH loss increased the bioenergetic capacity of HCT-116 cells (Fig.2E). Comparable results were observed in NT2197 cells (Supplementary Fig.2D-H). Collectively, these findings suggest that although ETF insufficiency limits the ability of cancer cells to utilize lipids and amino acids, it paradoxically upregulates their mitochondrial metabolism and bioenergetic capacity.

Glutamine plays an important role in fueling mitochondrial metabolism in cancer cells [13]. ETFDH abrogation increased glutamine uptake and glutamate production in both HCT-116

(Fig.2F) and NT2197 (Supplementary Fig.2I) cells. ETFDH loss increased ^{13}C-glutamine incorporation in the forward direction (green) and the reverse direction (purple) of the citric acid cycle (CAC; Fig.2G-H, Supplementary Fig.2J), suggesting higher glutamine utilization in the CAC, as well as increased reductive glutamine metabolism. Accordingly, ETFDH KO HCT-116 cells exhibited greater sensitivity to glutamine deprivation than control WT EV cells (Fig.2I). These findings show that ETFDH loss elevates glutamine utilization in the CAC to support mitochondrial metabolism. Collectively, these data demonstrate that ETF insufficiency in cancer cells remodels mitochondrial metabolism while increasing the bioenergetic capacity.

ETFDH loss induces intracellular accumulation of amino acids, mTOR signaling and protein synthesis

Consistent with the established role of ETFDH in amino acid catabolism [2], and reduction of leucine consumption upon ETFDH abrogation (Supplementary Fig.2C), steady state levels of most intracellular amino acids were increased in ETFDH KO vs. WT HCT-116 and NT2197 cells (Fig.3A). Moreover, ETFDH-deficient HCT-116 cells exhibited higher rates of protein synthesis relative to ETFDH-proficient cells (Fig.3B). Amino acids activate the mechanistic target of rapamycin (mTOR) which stimulates protein synthesis [14]. Indeed, mTORC1 signaling was higher in ETFDH-deficient than ETFDH-proficient HCT-116 and NT2197 cells as illustrated by increased phosphorylation of ribosomal protein S6 kinases (S6K1/2; Thr389) and their substrate ribosomal protein S6 (rpS6; Ser240/244) (Fig.3C). Re-expression of ETFDH in ETFDH KO cells resulted in normalization of mTORC1 signaling to the levels observed in WT EV cells (Fig 3D). mTORC2 signaling was also augmented upon ETFDH abrogation in HCT-116 and NALM6 cells as evidenced by increased AKT phosphorylation (Ser473) (Supplementary Fig.3A-B). Despite

bioenergetic rewiring, ETFDH loss did not exert a major effect on the activity of adenosine monophosphate-activated protein kinase (AMPK) as monitored by its phosphorylation (Thr172) or phosphorylation of its substrate acetyl-CoA carboxylase (ACC at S79) (Supplementary Fig.3A-B).

Consistent with mTOR hyperactivation, ETFDH KO HCT-116 cells were more sensitive to the active site mTOR inhibitor Torin1 [15] as compared to their ETFDH-proficient counterparts (Supplementary Fig.3C). To further determine which mTOR complex is responsible for mediating the hyper-proliferative phenotype triggered by ETFDH loss, we selectively inactivated mTORC1 or mTORC2 by depleting RAPTOR or RICTOR, respectively using small hairpin RNA (shRNA) in WT and ETFDH KO HCT-116 cells (Supplementary Fig.3D). Depletion of RAPTOR, but not RICTOR strongly attenuated the proliferation of ETFDH KO cells (Supplementary Fig.3E-F). Moreover, the anti-proliferative effects of bisteric mTORC1-specific inhibitor BiS-35x [16] were stronger in ETFDH KO vs. ETFDH Rescue HCT-116 cells (Supplementary Fig.3G). Altogether, these data suggest that mTORC1, but not mTORC2 acts as a major mediator of hyper-proliferative phenotype triggered by ETFDH loss in cancer cells. Accordingly, the effects of amino acid deprivation on phospho-rpS6 (Ser240/244), and phospho-4E-BP1 (Ser65) were attenuated in ETFDH KO vs. WT control cells, which is consistent with the intracellular accumulation of amino acids upon ETFDH disruption (Fig.3E-G). In turn, serum stimulation (Stim) resulted in comparable induction in phosphorylation of rpS6 (Ser240/244) and 4E-BP1 (Ser65) in ETFDH-deficient and proficient cells (Fig.3E). Collectively, these findings suggest that ETFDH loss induces mTORC1 signaling at least in part by increasing intracellular amino acid levels.

Amino acid deprivation leads to general control nonderepressible 2 (GCN2)-dependent phosphorylation of the alpha subunit of eIF2 and subsequent induction of activating transcription

factor 4 (ATF4) synthesis during the integrated stress response (ISR) [17]. Consistent with an increase in intracellular amino acid, phosho-eIF2α (S51) levels appeared to be modestly reduced in ETFDH-deficient vs. proficient HCT-116 cells under both serum starvation and amino acid depletion (Supplementary Fig.3H). However, the ETFDH status in the cells did not affect ATF4 levels at baseline or upon amino acid depletion (Supplementary Fig.3H). Altogether, these data demonstrate that ETFDH loss induces mTORC1 signaling and protein synthesis, which appears to be at least in part driven by intracellular accumulation of amino acids.

ETFDH loss diminishes 4E-BP1, but not 4E-BP2 protein levels

mTORC1 positively controls cell proliferation through the eukaryotic translation initiation factor 4E-binding proteins (4E-BPs; 4E-BP1-3 in mammals) [18]. Of note, 4E-BP3 is expressed in a tissue-restricted manner, and does not appear to play a major role in regulating proliferation [18]. mTORC1 phosphorylates 4E-BPs to promote eukaryotic translation initiation factor 4F (eIF4F) complex assembly by dissociating 4E-BPs from eIF4E, thereby stimulating cap-dependent translation initiation [19]. Consistent with the increased mTORC1 activity, ETFDH-deficient cells exhibited increased phosphorylation of 4E-BP1 (Ser65), which was rescued upon re-expression of ETFDH in HCT-116 and NT2197 cells (Fig.4A). Unexpectedly, we observed that ETFDH loss coincided with a dramatic reduction in total 4E-BP1 protein levels in HCT-116, NT2197 (Fig.4A), NALM6 (Supplementary Fig.4A), and 4T1 cells (Supplementary Fig.4B). We also treated WT and ETFDH KO HCT-116 cell lysates with λ-phosphatase to exclude potential confounding effects of different 4E-BP1 phosphorylation states, which confirmed that disruption of ETFDH is paralleled by reduction in 4E-BP1 levels (Fig.4B). Notably, loss of ETFDH did not exert a major effect on 4E-BP2 protein abundance in HCT-116 (Fig.4A), NT2197 (Fig.4A), or 4T1 cells (Supplementary

Fig.4B). In addition, 4E-BP1, but not 4E-BP2 protein levels were reduced in ETFDH-deficient HCT-116 as compared to WT tumors (Fig.4C-E). Strikingly, loss of ETFDH in non-transformed NMuMG cells did not exert a major effect on mTORC1 signaling (Supplementary Data Fig.4C) and failed to alter 4E-BP1 protein levels (Supplementary Fig.4C). Collectively, these findings indicate that ETF insufficiency is paralleled by a selective decrease in 4E-BP1 protein levels in cancer, but not non-transformed cells.

Decrease in 4E-BP1 protein levels underpins the bioenergetic rewiring induced by ETF insufficiency in cancer cells.

Considering that in mammals 4E-BPs play a major role in mediating the effects of mTORC1 on proliferation, neoplastic growth, mitochondrial functions and protein synthesis [18,20,21], we next investigated whether the observed decrease in 4E-BP1 levels contributes to increased proliferation and tumor growth caused by ETFDH abrogation. To this end, we overexpressed 4E-BP1 protein in ETFDH-deficient NT2197 cells by infecting them with a retrovirus wherein *EIF4EBP1* expression was driven by an exogenous promoter [18]. Importantly, 4E-BP1 overexpression in ETFDH KO NT2197 cells decreased eIF4F complex assembly, as evidenced by m^7-GTP pulldown (Fig.4F). 4E-BP1 overexpression also reduced oxygen consumption in ETFDH KO NT2197 cells, relative to empty vector infected cells (Fig.4G). Moreover, restoring 4E-BP1 protein levels decreased cell proliferation (Supplementary Fig.4D) and anchorage-independent growth (Supplementary Fig.4E) of ETFDH KO HCT-116 cells. Lastly, 4E-BP1 overexpression decreased growth and the final volume of tumors formed by NT2197 ETFDH KO cells in SCID-BEIGE mice (Fig.4H-I). Collectively, these data indicate that decreased 4E-BP1 protein levels mediate the pro-neoplastic effects of ETF insufficiency.

The mTORC1/4E-BP axis stimulates mitochondrial biogenesis and metabolism by altering the translation of nuclear-encoded mitochondrial mRNAs including mitochondrial transcription factor A (TFAM) [21,22]. ETFDH loss increased mitochondrial DNA levels (Fig.4J) and mass (Supplementary Fig.4F) which was paralleled by TFAM induction (Fig.4K). Collectively, these data show that the loss of 4E-BP1 plays a prominent role in mediating the effects of ETF insufficiency on bioenergetic reprogramming of cancer cells.

ETFDH loss decreases *EIF4EBP1* transcription via BCL-6

We next set out to determine the level(s) at which 4E-BP1 protein levels are downregulated in ETF insufficient cancer cells. ETFDH loss did not have a major effect on 4E-BP1 protein synthesis or turnover (Supplementary Fig.4G-H), but it decreased the *EIF4EBP1* mRNA levels in ETFDH-deficient vs. ETFDH-proficient HCT-116 (Fig.4L) and NT2197 cells (Fig.4M). *EIF4EBP1* and *ETFDH* mRNA levels were also positively correlated in tumors isolated from colorectal adenocarcinoma patients (Supplementary Fig.4I). In turn, consistent with no apparent differences in 4E-BP2 protein levels, the levels of *EIF4EBP2* mRNA were unaffected by the ETFDH status in both cell lines (Fig.4L-M). Notably, observed decrease in *EIF4EBP1* mRNA levels was not caused by the effects of ETFDH loss on mRNA stability (Supplementary Fig.4J). Based on these data, we concluded that ETFDH abrogation is paralleled by suppression of *EIF4EBP1* transcription and sought to identify transcription factors that may mediate the effects of ETFDH abrogation on suppression of *EIF4EBP1* expression. ATF4, Snail and Slug have been shown to stimulate transcription of *EIF4EBP1*, but not *EIF4EBP2* [23,24]. However, ATF4, Snail and Slug proteins remain unchanged upon ETFDH disruption (Supplementary Fig.3H, Supplementary Fig.5A). We also re-analyzed publicly available RNA-seq datasets, which revealed that

EIF4EBP1, but not *EIF4EBP2* expression was increased following STAT1 abrogation in MT4788 breast cancer cells [25]. Indeed, we observed that MT4788 STAT1 KO cells have increased 4E-BP1 protein levels relative to parental cells (Supplementary Fig.5B). Accordingly, ETFDH KO cells displayed increased STAT1 and downregulated 4E-BP1 protein levels (Supplementary Fig.5C). To determine the impact of STAT1 on *EIF4EBP1* or *EIF4EBP2* promoter occupancy, we performed chromatin immunoprecipitation qPCR (ChIP-qPCR) assay in control (WT EV), ETFDH KO, or ETFDH rescue HCT-116 cells (Supplementary Fig.5D-E). Binding of STAT1 was however comparable to IgG across all tested cell lines thereby suggesting that is unlikely that STAT1 directly suppresses *EIF4EBP1* transcription in the context of ETFDH loss (Supplementary Fig.5D-E). Furthermore, reactive oxygen species (ROS) can also influence redox-responsive transcription [26]. Although loss of ETFDH induced ROS levels (Supplementary Fig.5F), 4E-BP1 protein abundance was not altered following treatment with the antioxidant N-acetyl-cysteine (NAC) (Supplementary Data Fig.5G).

We next investigated the potential role of B-cell lymphoma 6 (BCL-6) [27-29], which was previously suggested to suppress *EIF4EBP1* transcription [30]. Notably, *ETFDH* abrogation in HCT-116 and NT2197 cells resulted in a marked increase in BCL-6 protein levels, compared to ETFDH-proficient control cells (Fig.5A). These changes in BCL-6 protein levels were mTOR-sensitive (Fig.5B) and not accompanied by the alterations in *BCL6* mRNA abundance (Fig.5C), which is consistent with recently reported mTOR-dependent translational activation of BCL-6 [31-33]. Indeed, *BCL6* mRNA translation was increased in HCT-116 ETFDH KO relative to WT cells (Fig.5D). Taken together, these data point out that ETFDH disruption induces BCL-6 protein synthesis in an mTOR-dependent manner. ETF insufficiency increased BCL-6 binding to the *EIF4EBP1*, but not the *EIF4EBP2* promoter (Fig.5E-F). BCL-6 silencing in NT2197 and 4T1 ETFDH KO cells

increased 4E-BP1 protein levels (Fig.5G-H). Depletion of BCL-6 also attenuated proliferation of 4T1 ETFDH KO cells (Fig.5I). Collectively, these findings show that BCL-6 mediates the effects of ETF insufficiency on reduction in *EIF4EBP1* expression and increased proliferation of cancer cells.

ETFDH acts as a haploinsufficient tumor suppressor.

Data available in cBioPortal from 2683 samples across cancer types [34] indicate that missense or truncating mutations in ETFDH are rare (0.3%) (Fig.6A). This suggests that ETFDH is not lost, but rather downregulated in human cancers. We observed that DNA methylation inhibitors, 5-azacytidine (5-aza) and 5-aza-2′-deoxycytidine (5-aza-2-deoxyC) increased ETFDH protein levels in HCT-116 cells (Fig.6B), thus suggesting that one of the potential mechanisms of downregulated *ETFDH* expression in neoplasia may stem from increased DNA methylation. Based on these observations, we developed a model that more closely reflects ETFDH downregulation, but not a complete loss, in human tumors using a method based on targeted poly(A) track insertion within endogenous genes [35]. The length of the poly(A) track directly correlates with the reduction in amount of protein produced, allowing for the investigation of gene-dosage effects on ensuing phenotypes [35,36]. Accordingly, mutants were designed by inserting poly(A) tracks of 12 and 18 adenosines [12A, equivalent to 4 consecutive AAA (Lys) codons $(AAA)_4$; 18A, equivalent to 6 consecutive AAA (Lys) codons $(AAA)_6$], as well as a control track (CTRL) [6 consecutive lysine AAG codons $(AAG)_6$] (Supplementary Fig.6A, see methods). Based on an Alphafold rendered structure (version 2) [37,38], we chose residue 38 in an unstructured loop as an insertion site (Supplementary Fig.6B). Of note, $(AAA)_6$ and $(AAG)_6$ stretches are translated in the equal number of Lys residues, whereby (AAA), but not (AAG), stretches decrease ETFDH protein levels

(Fig.6C). $(AAG)_6$ construct was thus used as a control to mitigate potential inadvertent effects of the insertion of poly-Lys on the ETFDH function. $(AAA)_4$ and $(AAA)_6$ stretches progressively reduced ETFDH protein abundance as compared to constructs harboring the $(AAG)_6$ track (Fig.6C). The reduction in ETFDH protein levels was mirrored by a gene-dose dependent increase in mTORC1 signaling, BCL-6 expression and reduction in 4E-BP1, but not 4E-BP2 protein levels (Fig.6C). Accordingly, *Eif4ebp1* mRNA levels were reduced in *ETFDH* dose-dependent manner, while *Eif4ebp2* mRNA levels remained unaffected (Fig.6D). Moreover, reduction in ETFDH protein levels correlated with increased mtDNA content (Fig.6E), oxygen consumption (Fig.6F), ATP production from OXPHOS (JATPox) (Fig.6G), bioenergetic capacity (Fig.6H), and cell proliferation (Fig.6I). Finally, ETFDH KO NT2197 tumors carrying $(AAA)_6$ insertions exhibit increased tumor growth and larger final tumor volumes relative to control tumors expressing $(AAG)_6$ insertions in SCID-BEIGE mice (Fig.6J-K). Altogether, these findings show that ETFDH gene-dosage influences neoplastic growth, thus suggesting that ETFDH may act as a haploinsufficient tumor suppressor.

Discussion

Notwithstanding that ETFDH mutations play a detrimental role in MADD metabolic disorders, we show that ETF insufficiency caused by reduced *ETFDH* expression plays a major role in rewiring cancer metabolism and signaling to stimulate neoplastic growth. Reduction of ETFDH levels appears to be a near-universal feature of cancer cells and is likely a consequence of DNA hypermethylation (Fig.6B), an event that is frequently observed among tumor suppressor genes [39]. Indeed, ETFDH was found among the most under-expressed metabolic enzymes in a study that compiled cancer microarray datasets [40]. Moreover, recent studies highlighted crosstalk between

aberrant mTOR signaling and epigenetic perturbations [41-44], which further reinforces the plausibility that epigenetic reprograming in cancer cells may underpin the pro-neoplastic role of ETFDH downregulation and/or explain resulting phenotypes.

Intriguingly, although ETF insufficiency limits the flexibility of cancer cells in using fuels (e.g., lipids and amino acids) for OXPHOS, it triggers retrograde signalling that established feed-forward loop via mTORC1 which leads to increased BCL-6 levels and reduced *EIF4EBP1* transcription (Fig.6L). ETF insufficiency thus orchestrates enhanced mTORC1 signaling with downregulation of 4E-BP1 protein levels to reprogram protein synthesis and ultimately increase mitochondrial biogenesis and functions thereby providing selective proliferative advantage to cancer cells (Fig.6L). To this end, ETF insufficiency allows cancer cells to trade of their metabolic flexibility for increased bioenergetic capacity and a re-wired signaling state that favors neoplastic growth. Importantly, while ETFDH plays an essential role in muscle, we did not observe a major effect of ETFDH disruption on proliferation, mTOR signaling or 4E-BP1 levels in non-transformed murine breast epithelial NMuMG cells. These observations suggest that ETF insufficiency causes remodeling of signaling and metabolic networks that are favourable to cancer cells.

Our findings are consistent with previously attributed tumor-suppressive effects of 4E-BP1 [45-50]. More recently, it has been demonstrated that under certain contexts 4E-BPs may play a beneficial role for tumor survival. For instance, 4E-BPs may facilitate tumor growth by regulating global and selective mRNA translation under periods of cellular stress [51,52], including suppression of fatty acid biosynthesis under glucose deprivation [53,54]. Collectively, these findings demonstrate that 4E-BPs are likely to play more complex, context dependent roles during cancer progression than previously anticipated. Moreover, the role of different 4E-BP proteoforms in cancer was in

general thought to be redundant. Our findings however demonstrate that in the context of ETF insufficiency selective decrease in 4E-BP1, but not 4E-BP2 levels plays a role in driving neoplastic growth thereby suggesting that 4E-BP1 and 4E-BP2 may play hitherto unappreciated non-overlapping roles in neoplasia.

In conclusion, we show that ETF insufficiency caused by reduced ETFDH expression causes retrograde signaling that remodels mitochondrial metabolism in a manner that drives neoplastic growth (Fig.6L), while either being neutral (NMuMG) or deleterious (muscle cells) in non-malignant cells. These findings explain how disruption of mitochondrial enzyme, rather than reducing cellular fitness, is common in cancer because it increases mitochondrial energy flux to drive neoplastic growth.

Figure 1: ETFDH loss promotes tumor growth

A) ETFDH protein levels in non-adjacent tissue (NAT) or grade 3 cancerous tissue (Tumor) were determined by immunocytochemistry (IHC) of colorectal cancer tissue microarray. Staining intensity of DAB in arbitrary units (A.U) is shown. Data are presented as means +/- SEM (NAT n=14, Tumor n=13), **$p<0.01$, unpaired Student's *t* test.

B-C) Tumor growth of WT EV, ETFDH KO, and ETFDH Rescue HCT-116 cells following intra-caecal injection (B) and endpoint tumor volumes (C). Growth was assessed by luminescence (photons). Data are presented as means +/- SEM (WT EV n=6, ETFDH KO n=8, ETFDH Rescue n=8), *$p<0.05$, one-way ANOVA, Tukey's post-hoc test.

D-E) Tumor growth of WT and ETFDH KO NT2197 cells following mammary fat-pad injection (D) and endpoint tumor volumes (E). Growth was assessed using a caliper. Data are presented as means +/- SEM (WT n=17, ETFDH KO n=17), *$p<0.05$, unpaired Student's *t* test.

Figure 2: Absence of ETFDH promotes mitochondrial metabolism

A-B) Oxygen consumption (A) and extracellular acidification (B) in WT EV, ETFDH KO, and ETFDH Rescue HCT-116 cells were determined using a Seahorse bioanalyzer. Data are normalized to cell count and presented as means +/- SD (n=4), *p<0.05, **p<0.01, one-way ANOVA, Tukey's post-hoc test.

C) Basal *J* ATP calculations from WT EV, ETFDH KO, and ETFDH Rescue HCT-116 cells. *J* ATP ox represents ATP production from oxidative phosphorylation, while *J* ATP glyc is ATP production from glycolysis. Comparison between *J* ATP ox (grey bars; top) and *J* ATP glyc (white bars; bottom) is shown. Data are presented as means +/- SD (n=4), *p<0.05, **p<0.01, one-way ANOVA, Tukey's post-hoc test.

D-E) Bioenergetic plot for Basal, FCCP, and Monensin *J* ATP fluxes (D) and bioenergetic capacity (E) of WT EV, ETFDH KO, and ETFDH Rescue HCT-116 cells. Data are presented as means +/- SD (n=4), *p<0.05, one-way ANOVA, Tukey's post-hoc test.

F) Glutamine uptake and glutamate production in WT and ETFDH KO HCT-116 cells. Results are shown as fold changes of ETFDH KO cells relative to WT cells. Data are presented as means +/- SD (n=3), *p<0.05, paired Student's *t* test.

G) Schematic of ^{13}C-glutamine tracing throughout the citric acid cycle (CAC). Isotopomers labelled in green depict ^{13}C-glutamine tracing in the forward direction of the CAC, while those in purple represent reverse tracing.

H) Relative abundance of ^{13}C-labelled metabolites in the forward (green) and reverse (purple) directions from WT (blue) and ETFDH KO (red) NT2197 cells. Data are presented as means +/- SD (n=3), *p<0.05, **p<0.01, ***p<0.001, ****p<0.0001, paired Student's *t* test.

I) Proliferation of WT and ETFDH KO HCT-116 cells grown in the absence or presence of glutamine for 48 hours. Results are shown as fold changes of cell counts under glutamine deprivation relative to those under glutamine repleted conditions. Data are presented as means +/- SD (n=3), *$p<0.05$, paired Student's *t* test.

Figure 3: ETFDH loss bolsters mTORC1 signaling and downregulates 4E-BP1 protein levels.

A) Amino acid profile in WT and ETFDH KO HCT-116 and NT2197 cells. Data are presented as fold change in amino acid levels in ETFDH KO compared to WT cells (n=3).

B) Puromycin incorporation assays in WT and ETFDH KO HCT-116 cells. Levels and phosphorylation status of indicated proteins were determined via western blotting using indicated antibodies. β-Actin was used as a loading control (representative blots of n=3). Quantification of puromycin incorporation is presented as fold change in ETFDH KO vs. WT cells.

C) Levels and phosphorylation status of indicated proteins in WT or ETFDH KO HCT-116 and NT2197 cells were determined by western blotting. β-Actin served as a loading control (representative blots of n=3).

D) Levels and phosphorylation status of indicated proteins in WT EV, ETFDH KO, or ETFDH Rescue HCT-116 and NT2197 cells were determined by western blotting. β-Actin was used as a loading control (representative blots of n=3).

E) Total and phosphoprotein levels in WT or ETFDH KO HCT-116 cells were determined by western blotting using indicated proteins. Cells were serum starved overnight, then depleted of amino acids for indicated timepoints (0, 10, 30, 60 minutes), or stimulated with FBS for 4 hours (Stim). β-Actin was used as loading control (representative blots of n=3).

F) Quantification of pS6(S240/244)/S6 ratio from data presented in panel E. Data are presented as means +/- SD (n=3), *$p<0.05$, one-way ANOVA, Tukey's post-hoc test.

G) Quantification of p4E-BP1(S65)/4E-BP1 ratio from data presented in panel E. Data are presented as means +/- SD (n=3), *$p<0.05$, one-way ANOVA, Tukey's post-hoc test.

Figure 4: Repression of *EIF4EBP1* transcription mediates the effects of ETFDH loss on cancer bioenergetics and tumor growth

A) Levels and phosphorylation status of indicated proteins in WT EV, ETFDH KO, or ETFDH Rescue HCT-116 and NT2197 cells were determined by western blotting. β-Actin was used as a loading control (representative blots of n=3).

B) Levels of indicated protein in λ-phosphatase treated WT or ETFDH KO HCT-116 and NT2197 cell lysates were monitored by western blotting. β-Actin was used as a loading control (representative blots of n=3).

C) Indicated protein levels in WT or ETFDH KO HCT-116 tumors were determined by western blotting. AKT was used as loading control (WT n=8, ETFDH KO n=11).

D-E) Quantification of 4E-BP1 (D) and 4E-BP2 (E) from tumors described in panel C. Data are presented as means +/- SEM (WT n=8, ETFDH KO n=11), ***$p<0.001$, unpaired Student's *t* test.

F) m^7GDP pulldown assay in ETFDH KO and ETFDH KO overexpressing 4E-BP1 (ETFDH KO 4E-BP1) NT2197 cells. Specified protein levels in m^7GDP pulldown or input were determined by western blot. β-Actin was used as loading control (input) and to exclude contamination in the pulldown material (m^7GTP bound) (representative blots of n=3).

G) Oxygen consumption of ETFDH KO and ETFDH KO 4E-BP1 NT2197 cells. Data are normalized to cell count and presented as means +/- SD (n=5), **$p<0.01$, Student's *t* test.

H-I) Tumor growth of ETFDH KO and ETFDH KO 4E-BP1 NT2197 cells following mammary fat-pad injection (H) and endpoint tumor volumes (I). Growth was assessed using caliper measurements. ETFDH KO measurements are the same as in Fig.1D, as these growth curves were obtained in the same experiment. Data are presented as means +/- SEM (ETFDH KO n=17, ETFDH KO 4E-BP1 n=18), **$p<0.01$, unpaired Student's *t* test.

J) Mitochondrial DNA in WT EV, ETFDH KO, and ETFDH Rescue HCT-116 cells was quantified by qPCR. Mitochondrial DNA (mtDNA) content was normalized to genomic DNA (gDNA). Data are presented as fold change relative to WT EV cells +/- SD (n=3), *p<0.05, **p<0.01, one-way ANOVA, Tukey's post-hoc test.

K) Levels of indicated proteins in WT EV, ETFDH KO, and ETFDH Rescue HCT-116 cells were assessed by western blotting. β-Actin was used as a loading control (representative blots of n=3).

L) *EIF4EBP1* and *EIF4EBP2* mRNA levels in WT EV, ETFDH KO, and ETFDH Rescue HCT-116 cells were determined by RT-qPCR. *PP1A* was used as a house-keeping gene. Data are presented as fold change of *EIF4EBP1/PP1A* and *EIF4EBP2/PP1A* ratios relative to WT EV cells (set to 1) +/- SD (n=3), *p<0.05, one-way ANOVA, Tukey's post-hoc test.

M) *Eif4ebp1* and *Eif4ebp2* mRNA abundance in WT and ETFDH NT2197 KO cells was determined by RT-qPCR. *Actb* was used as a house-keeping gene. Data are presented as fold change in *Eif4ebp1/Actb* and and *Eif4ebp2/Actb* ratios relative to WT cells +/- SD (n=3), *p<0.05, paired Student's *t* test.

Figure 5: Loss of ETFDH increases BCL-6 levels leading to BCL-6-dependent inhibition of *EIF4EBP1* transcription.

A) Levels of indicated proteins in WT or ETFDH KO HCT-116 and NT2197 cells were determined by western blotting. β-Actin was used as a loading control (representative blots of n=3).

B) Levels of indicated proteins in ETFDH KO NT2197 cells treated with DMSO or Torin1 (250nM) for 4 hours were determined by western blotting. β-Actin was used as a loading control (representative blots of n=3).

C) *BCL6/Bcl6* mRNA abundance in WT and ETFDH KO HCT-116 and NT2197 cells was determined by RT-qPCR. *PP1A* mRNA was used as a control for HCT-116 experiments, while *Actb* mRNA was used as a control for NT2197 experiments. Data are presented as fold change in *EIF4EBP1/PP1A* and *EIF4EBP2/PP1A* (HCT-116) and *Eif4ebp1/Actb* and and *Eif4ebp2/Actb* (NT2197) ratios relative to WT cells +/- SD (n=3), paired Student's *t* test.

D) Polysome profiling of WT and ETFDH HCT-116 KO cells. The absorbance at 254nm (AU 254nm) was used to monitor distribution of the 40S-, 60S- ribosomal subunits, monosomes (80S) and polysomes across the gradient. *BCL6* mRNA abundance from polysome gradient fractions was obtained using RT-qPCR. Data are shown as a mean percentage of mRNA in each fraction relative to cumulative corresponding mRNA amount across the whole gradient +/-SD (n=3).

E-F) Binding events of BCL-6 to the promoters of *EIF4EBP1* and *EIF4EBP2* were determined by ChIP-qPCR. IgG was used a negative control. Data are presented as % of input (n=3), *$p<0.05$, two-way ANOVA, Dunnett's post-hoc test.

G) The levels of indicated proteins in ETFDH KO NT2197 cells transfected with siRNA targeting BCL-6 (siBCL-6) or control, scrambled siRNA (siCTRL) were determined by western blotting. β-Actin was used as loading control (representative blots of n=2).

H) Levels of indicated proteins in ETFDH KO 4T1 cells infected with shRNAs targeting BCL-6 (shBCL-6 #1 or shBCL-6#2) or control, scrambled shRNA (shCTRL) were monitored by western blotting. β-Actin served as loading control (representative blots of n=3).

I) Proliferation of ETFDH KO shCTRL, shBCL-6 #1, or shBCL-6#2 4T1 cells. Data are presented as cell count means (n=3), *$p<0.05$, one-way ANOVA, Dunnett's post-hoc test.

Figure 6: Reduced expression of ETFDH increases mitochondrial metabolism and tumor growth

A) ETFDH mutations from 2683 samples across multiple cancer types. Number of missense and truncating mutations are shown relative to samples with no mutations. Data are acquired from the ICGC/TCGA Pan-Cancer Analysis of Whole Genomes Consortium [34], accessed from the cBioPortal server (www.cbioportal.org).

B) Levels of indicated proteins in WT HCT-116 cells treated with 2.5µM 5-azacytidine (5-aza), 10µM 5-aza-2' -deoxycytidine (5-aza-2-deoxyC), or a vehicle (DMSO) for 72 hours were determined by western blotting. β-Actin was used as a loading control (representative blots of n=3).

C) Levels and the phosphorylation status of indicated proteins in ETFDH KO NT2197 cells expressing ETFDH harboring $(AAG)_6$, $(AAA)_4$, $(AAA)_6$ tracks were determined by western blotting. β-Actin was used as a loading control (representative blots of n=3).

D) *Eif4ebp1* and *Eif4ebp2* mRNA abundance in $(AAG)_6$, $(AAA)_4$, and $(AAA)_6$ NT2197 cells were determined by RT-qPCR. *Actb* was used as a house-keeping gene. Data are presented as fold change in *Eif4ebp1/Actb* and *Eif4ebp2/Actb* ratios relative to $(AAG)_6$ NT2197 cells (n=3), *p<0.05, **p<0.01, one-way ANOVA, Dunnett's post-hoc test.

E) Mitochondrial DNA content in $(AAG)_6$, $(AAA)_4$, and $(AAA)_6$ NT2197 cells were monitored by qPCR. Mitochondrial DNA (mtDNA) content was normalized to genomic DNA (gDNA) content. Data are presented as mean fold change relative to $(AAG)_6$ NT2197 cells -/+ SD (n=3), *p<0.05, **p<0.01, one-way ANOVA, Dunnett's post-hoc test.

F) Oxygen consumption of $(AAG)_6$, $(AAA)_4$, and $(AAA)_6$ NT2197 cells was determined using Seahorse bioanalyzer. Data are normalized to cell count and presented as means +/- SD (n=4), one-way ANOVA, Dunnett's post-hoc test.

G-H) Bioenergetic Plot for Basal, FCCP, and Monensin *J* ATP fluxes (G) and Bioenergetic Capacity (H) derived from $(AAG)_6$, $(AAA)_4$, and $(AAA)_6$ NT2197 cells. Data are presented as means +/- SD (n=4), one-way ANOVA, Dunnett's post-hoc test.

I) Proliferation of $(AAG)_6$, $(AAA)_4$, and $(AAA)_6$ NT2197 cells. ETFDH rescue measurements are the same as in Supplementary Fig.1F. Data are presented as cell count means +/- SD (n=4), **p<0.01, one-way ANOVA, Dunnett's post-hoc test.

J-K) Tumor growth of $(AAG)_6$ and $(AAA)_6$ NT2197 cells following mammary fat-pad injection (J) and endpoint tumor volumes (K). Growth was assessed using calipers. Data are presented as means +/- SEM ($(AAG)_6$ n=6-12, $(AAA)_6$ n=11-13), **p<0.01, unpaired Student's *t* test.

L) Schematic representation of the model whereby reduction in ETFDH levels accelerates tumor growth. Reduction of ETFDH triggers accumulation of intracellular amino acids thus increasing mTORC1 signaling. This is orchestrated with BCL-6-dependent reduction in 4E-BP1 levels to drive mitochondrial biogenesis and increase bioenergetic capacity of cancer cells ultimately leading to more aggressive tumor growth.

Supplementary Figure 1: *ETFDH* expression is reduced across a broad array of cancer subtypes, whereby *ETFDH* is a non-essential gene in cancer cells.

A) Schematic of electron transfer from fatty and amino acids towards the electron transport chain (ETC) via electron transfer flavoprotein (ETF) and electron transport flavoprotein dehydrogenase (ETFDH).

B) Gene essentiality in NALM6 cells. 19084 genes are presented and ranked based on essentiality (1 being most essential and 19084 being the least essential). Orange bar depicts essential genes and grey bar depicts non-essential genes. The rank of *ETFDH* is compared to those of *MYC*, *NRAS*, *RB1*, and *TP53*.

C) *ETFDH* mRNA abundance profiles across tumor samples (red) compared to normal tissues (blue). Data are presented as log2CPM (counts per million). Data were derived from The Cancer Genome Atlas (TCGA) repository and accessed on the GEPIA2 server (http://gepia2.cancer-pku.cn) (Colon Adenocarcinoma: Normal n=349, Tumor n=275; Liver Hepatocellular Carcinoma: Normal n=160, Tumor n=369; Rectal Adenocarcinoma: Normal n=318, Tumor n=92; Ovarian Serous Cystadenocarcinoma: Normal n=88, Tumor n=426; Skin Cutaneous Melanoma: Normal n=558, Tumor n=461; Testicular Germ Cell Tumors: Normal n=165, Tumor n=137; Uterine Carcinoma: Normal n=78, Tumor n=57), $p<2.2x10^{-16}$.

D) *ETFDH* mRNA levels across healthy (labelled as normal) and breast tumor (labelled as tumor) samples. RNAseq data from both TCGA and GTex databases were processed and normalized as described. TPM values were downloaded from GEO [GSE86354 (healthy) and [GSM1536837 (tumour)]. Expression is presented as log_2 standardised mRNA levels. Data were acquired from the 'Breast cancer gene-expression miner' (bc-GenExMiner) server

(http://bcgenex.ico.unicancer.fr) using *ETFDH* expression according to nature of the tissue. (Normal n=92, Tumor n=743). $p<0.0001$, Dunnett-Tukey-Kramer's test.

E-F) Proliferation of WT EV, ETFDH KO, and ETFDH Rescue HCT-116 (E) and NT2197 (F) cells. ETFDH rescue measurements are the same as in Fig.6I. Data are presented as cell count means +/- SD over multiple time-points. Representative western blot of indicated proteins is provided in the inlets (n=3), *$p<0.05$, **$p<0.01$, one-way ANOVA, Tukey's post hoc test.

G-H) Proliferation of WT and ETFDH KO 4T1 (G) and NALM6 (H) cells. Data are presented as cell count means +/- SD over indicated time-points. Representative western blot of indicated proteins is provided in the inlets (n=3), *$p<0.05$, paired Student's *t* test.

I) Proliferation of WT and ETFDH KO NMuMG cells. Representative western blot of indicated proteins is provided in the inlets (n=3), one-way ANOVA, Dunnett's post hoc test.

J) Soft agar/colony formation assays in WT EV, ETFDH KO, and ETFDH Rescue HCT-116 cells. Data are presented as fold change relative to WT EV cells (n=3), *$p<0.05$, **$p<0.01$, one-way ANOVA, Tukey's post-hoc test.

Supplementary Figure 2: ETFDH loss reprograms mitochondrial bioenergetics

A) Schematic depicting fatty acid and leucine catabolism linked to ETFDH electron transfer.

B) Palmitate oxidation at basal level in WT EV, ETFDH KO, and ETFDH Rescue HCT-116 cells. Data are presented as means +/- SD (n=6), ****p<0.0001, one-way ANOVA, Tukey's post-hoc test.

C) Fractional enrichment (%) of citrate m+2 in WT EV, ETFDH KO, and ETFDH Rescue HCT-116 cells. Data are presented as means +/- SD (n=6), ****p<0.0001, one-way ANOVA, Tukey's post-hoc test.

D-E) Oxygen consumption (D) and extracellular acidification (E) for WT and ETFDH KO NT2197 cells was determined using a Seahorse bioanalyzer. Data are normalized to cell count and presented as means +/- SD (n=5), *p<0.05, **p<0.01, paired Student's *t* test

F) Basal *J* ATP calculations from WT and ETFDH KO NT2197 cells. *J* ATP ox represents ATP production from oxidative phosphorylation, while *J* ATP glyc is ATP production from glycolysis. Comparison between *J* ATP ox (grey bars; top) and *J* ATP glyc (white bars; bottom) is shown. Data are presented as means +/- SD (n=5), ***p<0.001, paired Student's *t* test.

G-H) Bioenergetic Plot for Basal, FCCP, and Monensin *J* ATP fluxes (G) and Bioenergetic Capacity (H) for WT and ETFDH KO NT2197 cells. Data are presented as means +/- SD (n=5), *p<0.05, paired Student's *t* test.

I) Glutamine uptake and glutamate production in WT and ETFDH KO NT2197 cells. Data are presented as mean fold changes of ETFDH KO cells relative to WT cells +/- SD (n=3), *p<0.05, paired Student's *t* test.

J) Fractional abundance of ^{13}C-labelled metabolites over indicated timepoints from WT (blue) and ETFDH KO (red) NT2197 cells. Isotopomers labelled in green depict ^{13}C-glutamine tracing in the

forward direction of the CAC, while those in purple represent reverse tracing. Data are presented as means +/- SD (n=3), *p<0.05, **p<0.01, ***p<0.001, ****p<0.0001, two-way ANOVA, Tukey's post hoc test.

Supplementary Figure 3: ETFDH loss increases mTORC1 signaling and dependency

A-B) Levels and phosphorylation status of indicated proteins in WT and ETFDH KO HCT-116 (A) and NALM6 (B) cells were determined by western blotting. β-Actin was used as a loading control (representative blots of n=3).

C) Proliferation of HCT116 ETFDH KO and ETFDH Rescue cells treated with indicated concentrations of Torin1 for 72h. Data are presented as fold changes relative to vehicle (DMSO) treatment (n=3), *p<0.05, **p<0.01, ***p<0.01, two-way ANOVA, Tukey's post hoc test.

D) Indicated protein levels in WT and ETFDH KO HCT-116 cells transfected with shRNA targeting *RAPTOR* (shRAPTOR), *RICTOR* (shRICTOR), or scrambled control (SCR) were determined by western blotting. β-Actin was used as a loading control (representative blots of n=3).

E-F) Proliferation of HCT-116 WT and ETFDH KO cells expressing SCR and shRAPTOR (E) or SCR and shRICTOR (F). Data are presented as cell count means +/- SD (n=4), **p<0.01, ***p<0.01 two-way ANOVA, Tukey's post hoc test.

G) Proliferation of HCT116 ETFDH KO and ETFDH Rescue cells treated with indicated concentrations of BiS-35x for 72 hours. Data are presented as fold changes relative to vehicle (DMSO) treatment (n=3), *p<0.05, **p<0.01, ***p<0.01, two-way ANOVA, Tukey's post hoc test.

H) Total and phosphoprotein levels in WT or ETFDH KO HCT-116 cells were determined by western blotting using indicated proteins. Cells were serum starved overnight, then depleted of amino acids for indicated timepoints (0, 10, 30, 60 minutes), or stimulated with FBS for 4 hours (Stim). β-Actin was used as loading control (representative blots of n=3).

Supplementary Figure 4: *ETFDH* loss induces *EIF4EBP1* transcription

A) Protein levels in WT and ETFDH KO NALM6 cells were monitored by western blotting using indicated antibodies. β-Actin was used as a loading control (representative blots of n=3).

B) Indicated protein levels in WT and ETFDH KO 4T1 cells were determined by western blotting using indicated antibodies. β-Actin was used as a loading control (representative blots of n=3).

C) Protein levels in WT and ETFDH KO NMuMG cells were monitored by western blotting using indicated antibodies. β-Actin was used as a loading control (representative blots of n=3).

D) Proliferation of ETFDH KO and ETFDH KO overexpressing 4E-BP1 (ETFDH KO 4E-BP1) HCT-116 cells. Data are presented as cell count means +/- SD over indicated time-points (n=3), **$p<0.01$, paired Student's *t* test.

E) Soft agar/colony formation assay in ETFDH KO and ETFDH KO 4E-BP1 HCT-116 cells. Data are presented as fold change relative to ETFDH KO cells (n=3), *$p<0.05$, paired Student's *t* test.

F) Mitochondrial mass in WT and ETFDH KO NT2197 cells was monitored by flow cytometry. Data are presented as fold change relative to WT cells (n=3), **$p<0.01$, paired Student's *t* test.

G) The levels of indicated proteins in WT and ETFDH KO HCT-116 cells treated with cycloheximide (CHX) (50μg/ml), MG-132 (10μM), or combination thereoff for 4 hours total were monitored by western blotting. β-Actin was used as loading control, whereas p21 was used as a short-lived protein to control for the effects of the CHX and MG-132 treatments (representative blots of n=2).

H) Polysome profiling of WT and ETFDH HCT-116 KO cells. Absorbance at 254nm (AU 254nm) was used to monitor the distribution of 40S-, 60S- ribosomal subunits, monosomes (80S) and polysomes across the gradient. Indicated mRNA abundances from polysome gradient fractions

was obtained using RT-qPCR. Data are shown as a mean percentage of mRNA in each fraction relative to cumulative corresponding mRNA amount across the whole gradient +/-SD (n=3).

I) Correlation between *ETFDH* and *EIF4EBP1* mRNA expression in colon adenocarcinoma samples. Data were derived from TCGA repository.

J) WT and ETFDH KO HCT-116 cells were treated with Actinomycin D (10µg/ml) for indicated timepoints upon which *EIF4EBP1* and *GAPDH* mRNA levels were determined by RT-qPCR. Data are presented as a mean percentage of mRNA relative to DMSO-treated cells +/-SD (n=3).

Supplementary Figure 5: The effects of ETFDH loss on *EIF4EBP1* transcription are mediated by BCL-6 but not STAT1, Snail or Slug

A) Protein levels in WT and ETFDH KO HCT-116 cells were determined by western blotting using indicated antibodies. β-Actin was used as a loading control (representative blots of n=2).

B) MT4788 WT and STAT1 KO cells were treated with IFNγ (1ng/µl) to induce STAT1 or vehicle (water) for 24 hours. Levels and phosphorylation status of indicated proteins were determined by western blotting. β-Actin was used as a loading control (representative blots of n=2).

C) Protein levels in WT and ETFDH KO HCT-116 cells were assessed by western blotting using annotated antibodies. β-Actin served as a loading control (representative blots of n=3).

D-E) Binding of STAT1 to the promoters of *EIF4EBP1* (D) and *EIF4EBP2* (E) was determined by ChIP-qPCR. IgG was used a negative control. Data are presented as a percentage of the input +/- SD (n=3), one-way ANOVA, Tukey's post-hoc test.

F) Fluorescence intensity of WT and ETFDH KO HCT-116 cells stained with DCFDA (2µM) and measured by flow cytometry. Median values are depicted in the inlets.

G) Levels of 4E-BP1 in WT and ETFDH KO HCT-116 cells were determined by western blotting using the indicated antibody. β-Actin was used as a loading control (representative blots of n=3).

Supplementary Figure 6: Poly(A) Track design

A) Insertion of poly(A) tracks within the coding sequence of murine ETFDH. DNA sequences for constructs $(AAG)_6$, $(AAA)_4$, $(AAA)_6$, and WT Etfdh are shown.

B) Protein structure of $(AAG)_6$ / $(AAA)_6$ constructs generated using AlphaFold.

Methods

Cell lines and cell culture

HCT-116, NALM6, and HEK293T cells were obtained from American Type Culture Collection (ATCC) and verified using ATCC Cell line authentication service. NMuMG, NT2197, and MT4788 Parental and STAT1 KO cells were obtained by Dr. J. Ursini-Siegel's lab, while 4T1 (4T1-526) cells were obtained from Dr. P.M. Siegel's group. HEK293T and HCT-116 cells were cultured in DMEM supplemented with 10% fetal bovine serum (FBS), 1% penicillin/streptomycin and supplemented with 2mM L-Glutamine to obtain a final concentration of 6mM L-Glutamine. NALM6 and 4T1 cells were cultured in RPMI-1640 supplemented with 10% FBS, 1% penicillin/streptomycin and 2mM L-Glutamine. NMuMG and NT2197 cells were cultured in DMEM supplemented with 10% FBS, 1% penicillin/streptomycin, 2mM L-Glutamine, 10 mg/mL insulin, 20 mM HEPES, pH 7.5. NT2197 culture media was supplemented with puromycin (2 μg/mL) as previously described [11]. MT4788 were grown in DMEM, 2.5% FBS, mammary epithelial growth supplement (MEGS), 1% penicillin/streptomycin and gentamycin as previously described [25]. All cell lines were maintained at 37°C and 5% CO2 in a humidified environment and tested periodically for mycoplasma according to the manufacturer's instructions.

Animals

6–8-week-old SCID-BEIGE mice were purchased from Charles River. Male SCID-BEIGE mice were used for intracaecal experiments, while female mice were used for mammary fat pad injections. All animal experiments were performed in accordance with the guidelines of the McGill University Animal Ethics Committee and the Canadian Council on Animal Care as approved by the facility animal care committee.

Xenograft Experiments

Luciferase-expressing HCT-116 cells (250,000 cells) were injected intracaecally in male (8-10 weeks old) SCID-BEIGE mice as previously described [55]. Tumor growth was monitored and assessed by luminescence (IVIS spectrum, PerkinElmer). Animals were sacrificed after 50 days. Quantification of signal intensity was performed with Living Image software (PerkinElmer). NT2197 mammary tumor cells (50,000 cells) were injected in mammary fat pads of 6-8-week female SCID-BEIGE mice. Tumor growth was monitored using calipers. Measurements were shown as once tumor volume reached 100∼200 mm^3 and animals were sacrificed before tumors reached 1cm^3. Tumors were excised, placed in 10% formalin, and embedded for immunohistochemistry.

Cell Proliferation Assay

Cells were counted using a Countess automated cell counter (Invitrogen) and trypan blue exclusion was used for determining cell viability. Cells (HCT-116, NT2197, NMuMG, 4T1, NALM-6, and MT4788) were seeded in 6-well dishes and counted to 3-5 days. For glutamine deprivation experiments, HCT-116 cells were seeded in full culture for 24 hours. The next day, cells were grown in media in the presence or absence of glutamine for 48 hours and then counted. For Torin1/BiS-35x treatment experiments, HCT-116 cells were seeded overnight. The next day, media was replaced with treatment media containing Torin1 (50nM, 100nM, 250nM, 500nM) or BiS-35X (1nM, 10nM, 100nM, 1000nM) or DMSO for 72 hours and then counted.

Immunohistochemistry

Immunohistochemical staining of colon human parafilm-embedded tissue array (TissueArray.com, CO992b) was performed as previously described [56]. Briefly, the tissue slide was baked for 55°C for 30 min followed by incubation in xylene (2× 5 min), 100% ethanol (2× 5 min), 95% ethanol (2× 5 min), 75% ethanol (1× 5min), and ddH_2O (2x 5min). The slide was submerged in 10mM sodium citrate buffer (pH 6.0), 0.05% Tween-20 and heat-induced epitope retrieval was carried out in a pressure cooker for 30 min. The slide was cooled for 20 min at room temperature, rinsed in ddH_2O for 5 min, and washed with 1xTBS + 0.3% Triton X-100 for 10 min, then 1xTBS for 5 min at room temperature. The slide was incubated in 3% H_2O_2 for 10 min at room temperature and washed with TBST (1xTBS + 0.1% Tween-20) for 5 min to inactivate peroxidases. A liquid blocker pen (PAP Pen, DAKO) was used to circle tissues on the slide. The TMA was blocked for 1 hour in room temperature in the presence of DAKO Protein Block-Serum Free (DAKO, Cat#X0909). The slide was incubated overnight at 4°C with the ETFDH antibody (1:500, ProteinTech 11109-1-AP). The next day, the slide was washed in TBST (3x 5min), and secondary incubation was performed for 30 min at room temperature with secondary antibody (Antibody background reducing diluent and HRP rabbit substrate (Cell Signaling, Cat#7074)). The slide was washed in TBST (3x 5min) and DAB (Di-amine-benzidine) peroxidase substrate (Vector, Cat# SK-4100) was applied to the slide for 5 min. Reaction was stopped by washing in ddH_2O for 5 min. The slide was counterstained with filtered hematoxylin for 20 sec and rinsed with ddH_2O for 5 min. The slide was placed in 75% ethanol (1 min), 95% ethanol (1 min), 100% ethanol (1 min) and xylene (2x 5min). The slide was mounted with a cytoseal at 60°C and dried in a fumehood overnight. Quantitation of sections was performed using Imagescope software (Aperio).

Western Blotting

Western blotting was performed as previously described [44]. Briefly, cells were washed twice with PBS and lysed with RIPA buffer (50 mM Tris-HCl pH 7.5, 150 mM NaCl, 0.5% sodium deoxycholate, 1 mM PMSF, 1 mM DTT, 1% NP40, 0.1% SDS), supplemented with 1X protease inhibitor (Roche) and 1x PhoSTOP (Roche). Lysates were cleared at 4°C (10min, 13,000rpm). Protein concentrations were determined using BCA kit (ThermoFisher). Lysates were mixed with 5x Laemmli buffer (60mM Tris-HCl (pH 6.8), 10% glycerol, 2% SDS, 5% 2-mercaptoethanol, 0.05% bromophenol blue) and boiled (95°C for 5min). Proteins were resolved by SDS-PAGE (Bio-Rad) and transferred via wet transfer apparatus (Bio-Rad) to nitrocellulose membranes (Amersham). Membranes were blocked in 5% skim milk (dissolved in TBST (0.1% Tween 20 in 1× TBS)) and incubated in primary antibodies overnight at 4°C. The next day, membranes were washed in TBST and incubated with HRP-conjugated secondary antibodies for 1 hour. Membranes were washed and applied with ECL (Bio-Rad) for 1min. Exposure was carried out on an Azure c300 (Azure Biosystems). Images were quantified by ImageJ and analysed using GraphPad Prism10. The list of primary antibodies is described in Supplementary Table 1.

For λ-phosphatase experiments, cells were lysed with RIPA and supplemented with 1X protease inhibitor, without 1x PhoSTOP. Protein samples were combined with NEBuffer for protein metallophosphatases (PMP), $MnCl_2$, and λ-protein phosphatase for 30min at 30°C according to the manufacturer's instructions (New England Biolabs).

Cap-Binding Pull-Down Assay

Assay was carried out as previously described [18]. Briefly, NT2197 cells were seeded overnight in 150mm plates. The next day, media was changed, and cells were washed with PBS and dissolved

in lysis buffer containing 50mM MOPS/KOH (7.4), 100mM NaCl, 50 mM NaF, 2mM EDTA, 2mM EGTA, 1% NP40, 1% sodium deoxycholate, 7 mM β-mercaptoethanol, supplemented with 1X protease inhibitor (Roche) and 1x PhoSTOP (Roche). Lysates were cleared at 4°C (10min, 16,000g). Protein concentrations in samples were elucidated by BCA (ThermoFisher). Samples were equilibrated for 20 min rotating at 4°C with m^7-GDP-agarose beads (Jena Bioscience), then washed in buffer containing 50mM MOPS/KOH (7.4), 100mM NaCl, 50 mM NaF, 0.5mM EDTA, 0.5 mM EGTA, 7 mM β-mercaptoethanol, 0.5 mM PMSF, 1mM Na_3VO_4 and 0.1mM GTP, by centrifugation (500g for 1min). Bound proteins were eluted from beads via boiling in loading buffer. Western blotting was performed on eluted proteins and input samples to assess for eIF4F complex formation using 4E-BP1, eIF4G1, eIF4E, and β-actin antibodies.

Flow Cytometry

NT2197 cells were seeded in 6-well dishes for 24 hours. The next day, cells were stained with 50nM MitoTracker Deep Red (ThermoFisher) for 15 minutes at 37°C in the dark. Cells were washed, counted, and 100,000 cells were dissolved in 500µl HBSS (Gibco). Samples were analyzed with the LSR Fortessa cytometer (Becton Dickinson, Mountain View, CA). Fluorescence intensity was detected by excitation at 644nm and acquisition on the 665/-A channel for MitoTracker Deep Red. ROS measurements were performed as previously described [56]. Briefly, cells were incubated with H_2DCFDA (Molecular Probes) for 30 minutes at 37°C. Cells were trypsinized, washed, and resuspended in 500µl HBSS. Samples were sorted on a BD FACS Canto II system. Fluorescence intensities were calculated by FlowJo (Tree Star, Inc.).

Mitochondrial DNA Quantitation

Quantitation of mitochondrial DNA was carried out as previously described [21]. HCT-116 or NT2197 cells were seeded in 6-well dishes for 24 hours. Genomic and mitochondrial DNA were extracted using PureLink Genomic DNA Mini Kit (ThermoFisher) and quantified by qPCR using SensiFAST™ SYBR® Lo-ROX kit (Bioline).

Polysome-Profiling Assay

Experiments were carried out as previously described [57]. Briefly, HCT-116 cells were seeded overnight in 150mm plates. The next day, cells were washed in PBS containing 100 µg/ml cycloheximide and lysed in hypotonic buffer (5 mM Tris-HCl [pH 7.5], 2.5 mM $MgCl_2$, 1.5 mM KCl, 100 µg/ml cycloheximide, 2 mM DTT, 0.5% Triton X-100, and 0.5% sodium deoxycholate). Samples were loaded onto 10%-50% wt/vol sucrose density gradients (20 mM HEPES-KOH pH 7.6, 100 mM KCl, 5 mM $MgCl_2$) and spun on a SW40Ti rotor (Beckman Coulter) at 4°C (36,000 rpm for 2 hours). Samples were fractionated and recorded at OD 254nm using an ISCO fractionator (Teledyne ISCO). RNA from fractions and input was extracted using TRIzol (ThermoFisher) according to the manufacturer's instructions. RNA from each fraction and input was isolated using TRIzol (Invitrogen) according to the manufacturer's instructions. RT-qPCR was performed on fractions and input RNA (refer to section "RNA extraction and RT-qPCR" for more information). Primers are listed in Supplementary Table 2.

Puromycilation Assay

HCT-116 cells were grown in 10cm dishes for 24 hours. The next day, cells were treated with puromycin (10ug/ml) for 20 minutes. Cells treated with DMSO were used as negative controls.

Cells were lysed and protein samples were quantified. Western blotting was performed (refer to "Western Blotting" section for more information) and membranes were incubated in anti-puromycin antibody (Millipore, Cat#MABE343). Quantification of bands was performed by ImageJ.

Stable Isotope Tracing

GC/MS quantification and stable isotope tracing analysis (SITA) was performed as previously described [58]. Briefly, NT2197 cells were seeded in 6-well dishes. Prior to ^{13}C-glutamine SITA experiments, culture media was replaced with one whose composition contains 6mM unlabelled glutamine for 2 hours. Afterwards, media was replaced with media containing 6mM labelled ([U-13C])-glutamine media (Cambridge Isotope Laboratories, MA, USA; CLM-1822; L-glutamine ([U-13C5]), 99%) for 5, 15, 30, and 60 minutes. For ^{13}C-leucine SITA experiments, culture media was replaced with one containing unlabelled leucine (0.105g/L) for 2 hours, then incubated in media containing labelled (0.105g/L) ([U-13C])-leucine media (Cambridge Isotope Laboratories, MA, USA; CLM-2262-H-0.1; L-leucine ([U-13C6]), 99%) for 24 hours. Both steady state and tracing samples were washed in cold saline solution (9g/L NaCl) and scraped off with 80% methanol. Samples were sonicated at 4°C for 10 minutes (high setting, 30 seconds on/30 seconds off cycles) to rupture cells. Lysates were centrifuged at 4°C (14000g,10 minutes), and supernatants were collected with addition of an internal standard (750ng myristic acid-D27). Samples were dried overnight at 4°C by speed-vac (Labconco). Dried pellets are resuspended in methoxyamine hydrochloride (10mg/ml), sonicated, and cleared for 10 minutes. Samples are heated 70°C for 30 minutes then applied with N-tert-butyldimethylsilyl-N- methyltrifluoroacetamide (MTBSTFA) at 70°C for 1 hour. Derivatized samples are injected into an Agilent 5975C GC/MS (Agilent

Technologies, CA, USA) using methods described previously [58]. ^{13}C-tracer samples were run in parallel with unlabelled samples. MassHunter software (Agilent) was used to carry out mass isotopomer distribution analyses, with metabolites normalized to myristic acid-D27 and cell number. Isotopic distributions were corrected for naturally occurring isotopes using an in-house algorithm [59].

RNA Extraction and RT-qPCR

HCT-116 and NT2197 cells were plated in 6-well dishes and extracted using TRIzol (Ambion) or Aurum Total RNA Mini Kit (Bio-Rad) following the manufacturers' instructions. cDNA was synthesized from purified RNA using SensiFAST cDNA Synthesis Kit (Bioline), as per manufacturer's protocol. RT-qPCR was performed using SensiFAST SYBR Lo-ROX kit (Bioline). Primer sequences are found in Supplementary Table 2.

Chromatin Immunopreciptation (ChIP)

Experiments were performed as previously described [44]. Briefly, HCT-116 cells were grown in 150mm dishes and fixed in 4% formaldehyde for 10 min, followed by centrifugation. Pellets were resuspended in ChIP-buffer (50 nM Tris (pH 8), 100 mM NaCl, 5 mM EDTA, 1X PMSF, 2 mM NaF, 0.25% NP-40, 0.25% Triton X-100, 0.25% Sodium Deoxycholate, 0.005% SDS) supplemented with 1x cOmplete protease inhibitor (Roche). Samples are sonicated using Sonic Dismembrator Model 500 (ThermoFisher) at 5 cycles at 20% power, 5 cycles at 25% power, 5 cycles at 30% power; each cycle is 10 sec. Lysates are spun at 4°C (14,000rpm, 10min) and protein concentration was measured from supernatants using the BCA kit (ThermoFisher). Samples were loaded onto Protein G Plus-Agarose Suspension Beads (Millipore) and pre-cleared at 4°C for 3

hours. Input samples were collected, and immunoprecipitation was performed with anti-BCL6 (Cell Signaling, #5650) or anti-IgG (Cell Signaling, #2729) on the remainder of the sample overnight at 4°C. The following day, samples were washed in three wash buffers (20 mM Tris (pH 8), 2 mM EDTA, 0.10% SDS, 1% Triton X-100 with 150/200/599mM for Wash1/2/3 buffers respectively), then a wash with LiCl buffer (10 mM Tris (pH 8), 1 mM EDTA, 0.25 M LiCl, 1% NP-40, 1% Sodium Deoxycholate), and two washes with TE buffer (10 mM Tris (pH 8), 1 mM EDTA). Samples were eluted in elution buffer (0.1 M NaHCO3, 1% SDS), and de-crossliked at 65°C overnight. The following day, proteinase K was applied to samples and heated at 42°C for 1 hour. DNA was purified and collected using DNA collection column (BioBasic). ChIP-qPCR was performed for *EIF4EBP1* and *EIF4EBP2* using sequences found in Supplementary Table 3.

Respirometry Assay

Oxygen consumption (OCR) and extracellular acidification rate (ECAR) were measured using Seahorse XFe24 and XFe96 analyzers (Agilent) with the Mito Stress Test (Agilent) and Palmitate Oxidation Assay (Agilent), according to the manufacturer's instructions. Briefly, HCT-116 and NT2197 cells were seeded in Seahorse culture plates (XFe24: 50,000 cells or XFe96: 20,000 cells) and incubated at 37°C. Cells were washed twice and incubated in assay media. For mito stress test experiments, assay media is composed of 10mM glucose, 2mM glutamine, and 1mM sodium pyruvate. Injections include oligomycin (1µM), FCCP (1µM), rotenone/antimycin A (1µM), and monensin (20µM). ATP production from OXPHOS (ATPox) or glycolysis (ATPglyc) were quantified using algorithms presented previously [60]. For palmitate oxidation assay, cells were seeded in substrate-limited media (DMEM, 1% FBS, 0.5mM glucose, 1mM glutamine, 0.5mM carnitine). The next day, cells are washed with FAO Buffer (includes 0.5mM glucose, 0.5mM

carnitine, and 5mM HEPES). Immediately prior to run, palmitate-BSA or BSA control is added to the cell media. Basal respiration was recorded. Values were normalized to cell counts.

Soft Agar/Colony Formation Assay

Experiments were conducted as previously shown [12]. Briefly, 6-well dishes are filled with a bottom layer solution (1:1; 1% noble agar and 2X culture media (2X DMEM, 20% FBS, 2% Pen/Strep/Glutamine)) per well. Dishes are incubated at room temperature for 30 min to allow solution to solidify. 5,000-10,000 HCT-116 and NT2197 cells are mixed 1:1 with 0.6% noble agar and 2X culture media. 1.5ml of this mixture is transferred on top of the solidified agar wells. Dishes are incubated at room temperature to allow the top layer to solidify. Cells are grown at 37°C until colony formation is present. Dishes were stained with nitroblue tetrazolium (Sigma), and colonies were counted.

Protein Stability Assay

HCT-116 cells were seeded in 10cm dishes. The next day, cells were treated with cycloheximide (CHX) (50µg/ml) or DMSO for 2 hours. Furthermore, cells were treated with the proteasomal inhibitor, MG-132 (10µM) or DMSO for 2 hours. Final time point for all conditions was 4 hours. Protein was extracted, quantified, and western blotting was performed for ETFDH, p21, 4E-BP1, or β-actin (refer to "Western Blotting" section for more information).

RNA Stability Assay

Assay was performed as previously described [61]. Briefly, HCT-116 cells were seeded in 6-well dishes. The next day, cells were treated with actinomycinD (ActD) for 2,4,8 and 24 hours. RNA

was extracted, cDNA was synthesized, and RT-qPCR was performed (refer to "RNA extraction and RT-qPCR" for more information).

Generation of ETFDH Knockout Cell Lines

To deplete endogenous ETFDH expression in HCT-116 and NALM6 cells, two guides RNA (gRNAs) targeting exon 6 and exon 9 of human ETFDH (against ETFDH sequences AGGTTGGCCGAATGCTAGGATGG and GATGTAGGGATACAAAAGGATGG) (refer to Supplementary Table 4 for gRNA sequences) were designed using CHOPCHOP (https://chopchop.cbu.uib.no/)[62] and purchased with the appropriate overhangs to be cloned into LentiCRISPRv2(GFP) (Addgene #82416). Cloning was carried out as previously described [63,64], with the following modifications: BsmBI-v2 (New England Biolabs) was used to digest the lentiCRISPRv2 plasmid; plasmid DNA was recovered using Zymoclean Gel DNA Recovery Kit (Zymo Research), and ligation was performed overnight at 4°C. Transformation of the ligated plasmid was carried out at 42°C in chemically competent Stbl3 cells (Fisher Scientific). Bacteria were plated on Lysogeny Broth (LB)-agar plates containing ampicillin (1 µg/mL) (BioBasic). Extraction of plasmid DNA was conducted using the QIAprep Spin Miniprep Kit (Qiagen) and samples were sequenced using primer for human U6 promoter (refer to Supplementary Table 5 for sequence). Nucleofection was used to deliver the validated lentiCRISPRv2 plasmids into HCT-116 and NALM6 cells. Transfections of the plasmids were carried out in Nucleofector cuvettes, according to the optimized protocols for NALM6 and HCT-116 cells (Lonza Bioscience), with 1×10^6 cells used and 1X PBS was used instead of the commercial 4-D Nucleofector solution. Post-nucleofection, cells were allowed to grow for 72 hours at 37°C, 5% CO_2, prior to cell sorting (BD FACSAria™ Fusion Flow Cytometer (BD Biosciences)). Cells expressing GFP were selected and

grown in 96-well plates containing conditioned media (45% filtered culture media, 45% fresh media, & 10% FBS). After two weeks, sorted clones were transferred into 24-well plates and later into 6-well plates to be collected and validated. Depletion of endogenous ETFDH protein levels in both HCT-116 and NALM-6 cells was initially confirmed by immunoblotting. Candidate clones with loss of ETFDH expression were kept for further validation. Moreover, the genomic DNA loci of candidate clones were sequenced and analyzed for insertion–deletion mutations (INDELs). Two sets of PCR primers were designed in regions flanking the CRISPR target sites (refer to Supplementary Table 5 for validation PCR sequences). Extraction of genomic DNA for each clone was carried out using the PureLink Genomic DNA Mini Kit (Fisher Scientific). Two rounds of polymerase chain reaction (PCR) on the extracted genomic DNA (35 PCR cycles with Set 1 followed by 45 PCR cycles with Set 2) were carried out and gel electrophoresis was utilized to separate the PCR products. The smaller PCR product for each clone was excised and purified using the Zymoclean Gel DNA Recovery Kit (Zymo Research). The products were sequenced, and chromatograms were analyzed for the presence of mutations causing a premature stop-codon or a frameshift. Insertion–deletion mutations (INDELs) in *ETFDH* were verified by PCR followed by sequencing, while the absence of ETFDH protein was confirmed by western blotting for HCT-116 cells and NALM6 cells.

To deplete ETFDH expression in NMuMG, NT2197 and 4T1 cells, two guides (gRNAs) targeting exon 2 of mouse Etfdh (against mEtfdh sequences 5'-ATTTTTATGCAGCGTATCACTGG-3' and 5'-GAACATCTTGGAGCACACAGAGG-3') were designed using CHOPCHOP and cloned in LentiCRISPRv2(GFP) (Addgene #82416) and sequenced as shown above. For lentiviral production, 2.5×10^5 HEK293T cells were seeded overnight in a 6-cm dish (Sarstedt). The next day, cells were co-transfected with 4µg of respective

lentiCRISPRV2 GFP plasmid containing either one of the gRNA inserts or empty-lentiCRISPRV2 GFP plasmid, 2.66µg of psPAX2 packaging plasmid (Addgene 35002), and 1.66 µg of pMD2.G plasmid (Addgene #12259) using the jetPRIME transfection reagent as described by the manufacturer's protocol (Polyplus transfection). Growth media was changed after 24 hours. After 48 hours, viral supernatant was filtered (0.45 µm filter; (Frogga Bio)), mixed 1:1 with fresh culture media, and applied to target cells grown in 6-well plates along with 8 µg/mL polybrene (Sigma-Aldrich). Cells were re-transduced the following two days with viral supernatant. Cells were allowed to recover for 48 hours post-transduction. Cells were sorted into 96-well plates (Sarstedt) and grown to generate stable cell lines, as shown above. Depletion of mouse Etfdh protein levels was initially confirmed via immunoblotting for NT2197, 4T1, and NMuMG. The presence of INDELs leading to a premature stop codon or frameshift was determined by sequencing as shown above. Two sets of PCR primers were designed in the regions flanking the CRISPR target sites (refer to Supplementary Table 5).

Generation of ETFDH Rescue Cell Lines

To rescue human ETFDH expression in HCT-116 cells, ETFDH(NM_004453) Human Tagged ORF was cloned into pLenti-ETFDH-C-Myc-DDK-P2A-Puro plasmid according to the manufacturer’s instructions (Origene). The resulting plasmid, pLenti-ETFDH-C-Myc-DDK-P2A-Puro, was transfected with psPAX2, pMD2.G into HEK293T cells with JetPrime reagent (Polyplus) according to the manufacturer’s instructions. Viral supernatants were filtered (0.45µM) and applied to HCT-116 ETFDH KO cells with polybrene (6µg/mL). After 6 hours, cells were re-infected overnight. After 2 days, selection with puromycin (4µg/ml) was performed for 72 hours.

Uninfected cells were selected with puromycin to serve as negative controls. The re-introduction of ETFDH expression or control plasmid in the knockout cells was confirmed via western blotting.

To rescue ETFDH expression in NT2197 ETFDH KO cells, a lentiviral plasmid conferring hygromycin B resistance and expressing mEtfdh with PAM site mutations or expressing an ORF-Stuffer was created using VectorBuilder (VB221206-1257xet and VB900123-2599cba respectively). Lentivirus production and transduction were carried out as previously mentioned for three consecutive days. After 48h of recovery, cells were selected with 1 mg/mL hygromycin B for 3 days. Cells were confirmed by western blotting.

Generation of Poly(A) Track ETFDH Variants

Mutants were designed by inserting poly(A) tracks of multiple adenosines: control track (CTRL) [6 consecutive lysine AAG codons $(AAG)_6$], 12 adenosines [12A, equivalent to 4 consecutive AAA (Lys) codons $(AAA)_4$; 18 adenosines [18A, equivalent to 6 consecutive AAA (Lys) codons $(AAA)_6$] within the rescue plasmid pLV[Exp]-Hygro-EF1A>mEtfdh. The polyA track insertion site was determined using AlphaFold (version 2) [37,38] to minimize unintended effects caused by the poly-lysine stretches on the possible mitochondrial import sequence. The polyA tracks were inserted following residue 38, in an unstructured loop of the Etfdh protein. Site-directed mutagenesis was performed using QuikChange II site-directed mutagenesis kit, according to the manufacturer's instructions (Agilent). Briefly, cycling parameters are followed as: Cycle 1: 95°C for 1min; Cycle 2: 95°C for 30 sec, 60°C for 30 sec, 68°C for 10min; Cycle 3: 68°C for 7min. The resulting plasmids were generated: pLV[Exp]-Hygro-EF1A>mEtfdh-AAG_6, pLV[Exp]-Hygro-EF1A>mEtfdh-AAA_4, pLV[Exp]-Hygro-EF1A>mEtfdh-AAA_6. To generate the poly(A) track Etfdh mutant lines in NT2197 cells (termed AAG_6, AAA_4, AAA_6), lentivirus production and

transduction into NT2197 ETFDH KO cells was carried out as previously mentioned for three consecutive days. After 48h of recovery, cells were selected with 1 mg/mL hygromycin B for 3-4 days. ETFDH expression was confirmed by western blotting.

Generation of Cells Expressing *EIF4EBP1*

pBABE-puro-EV and pBABE-puro-4E-BP1 plasmids were used to overexpress 4E-BP1 in HCT-116 ETFDH KO cells. Retrovirus production and transduction was carried out similarly to lentivirus production, except 2.66 μg of pUMVC packaging plasmid (Addgene #8449) was utilized instead of psPAX2. Following three consecutive days of viral transduction, cells were allowed to recover for 48h prior to selection with 2 μg/mL puromycin (Sigma-Aldrich) for 3 days. To overexpress 4e-bp1 in NT2197 ETFDH KO cells, plasmids containing m4e-bp1 or ORF-Stuffer were generated by VectorBuilder (VB221206-1246sbx & VB900123-2599cba). Lentivirus production and transduction was carried out as previously mentioned for three consecutive days prior to a 48h recovery period. After this period, selection with hygromycin B (1 mg/mL) was conducted for 5-7 days. Validation was observed by western blotting.

Generation of Knockdown Models by shRNA/siRNA

Knockdown using shRNA was performed as previously described [20]. For BCL6 knockdown experiments, the following shRNA vectors were used: pLKO.1 Non-Target shRNA Control (Sigma, SHC002), BCL6 shRNA #1 (Sigma, TRCN0000084654), or BCL6 shRNA #2 (TRCN0000084655). For RAPTOR/RICTOR knockdown experiments, the following shRNA vectors were used: scramble shRNA (Addgene, Plasmid #1864), RAPTOR_1 shRNA (Addgene, Plasmid #1857), and RICTOR_1 shRNA (Addgene, Plasmid #1853). Briefly, HEK293T cells

were transfected with psPAX2, pMD2.G or target pLKO.1 lentiviral shRNA vectors with JetPrime reagent (Polyplus) according to the manufacturer's instructions. Viral supernatants were filtered (0.45µM) and transferred to target cells with polybrene (6µg/mL). After 6 hours, cells were re-infected overnight. After 2 days, selection with puromycin (4µg/ml) was performed for 72 hours. Uninfected cells were selected with puromycin to serve as negative controls. Cells were seeded and processed for protein extraction or cell proliferation. Validation was confirmed by western blotting for *BCL6* knockdown and *RAPTOR* or *RICTOR* knockdown.

Knockdown using siRNA was performed as previously described [58]. Briefly, target cells were transfected for 24 hours with 50nM Silencer Negative Control No.1 (Thermofisher, AM4611) or BCL6 siRNA (Thermofisher, Cat#4390771) using JetPrime reagent (Polyplus) according to the manufacturer's instructions. Cells were re-transfected the next day for 24 hours, then processed for protein extraction. Validation was confirmed by western blotting.

Expression Profiles from TCGA/GTEx Databases

Expression of *ETFDH* and *EIF4EBP1* mRNA across both normal and tumor samples were obtained from The Cancer Genome Atlas (TCGA) and GTEx repositories. The expression data were normalized using the TMM (trimmed mean of M values) method and presented as log2 counts per million. Correlations between the genes were assessed using Pearson's correlation coefficient.

Quantification and Statistical Analysis

Statistical analysis was performed using GraphPad Prism 10. Data are presented as mean +/- SD of independent experiments, unless stated otherwise. Technical replicates were averaged from 2-

3 independent experiments. Details on data quantification, presentation, and statistical analysis are included in figure legends.

Data Availability

Plasmids generated in this study will be deposited to Addgene. The original data will be deposited and available at Mendeley Data. Metabolomics data is available at MetaboLights (MTBLS11048).

Acknowledgments

We are thankful to the members of all involved laboratories and Stephane Richard for helpful discussions. We thank Luc Choinière and Mariana Russo for assistance with metabolomic experiments and Christian Young for assistance with flow cytometry. This research was funded by the Terry Fox Foundation (TFF) Oncometabolism Team Grant (TFF-242122) to I.T., P.S, and M.P, and Canadian Institutes of Health Research (CIHR) (PJT-183843, PJT-479494) to I.T. Research in OL's lab is supported by grants from the Swedish Research Council (2020-01665), Swedish Cancer Society (22 2186), the Cancer Research Funds of Radiumhemmet (231263) and the Wallenberg Academy Fellow Program. L-M.P. acknowledges the funds from Queen's University. D.P. is supported by CIHR Postdoctoral Fellowship (MFE-171312), Cancer Research Society (CRS) The Next Generation of Scientists Award (NGS), and LDI Desjardins Fellowship Program. P.J. and H.K. are supported by Fonds de Recherche du Québec – Santé (FRQS) Fellowships. I.T. is supported by Canada Research Chair in Regulation of mRNA Translation and Metabolism. Metabolic analysis was performed at the Rosalind and Morris Goodman Cancer Research Centre's Metabolomics Core Facility, which is supported by the Canada Foundation for

Innovation, the Dr. John R. and Clara M. Fraser Memorial Trust, the Terry Fox Foundation (TFF Oncometabolism Team Grant; TFF-242122), and McGill University.

Author Contributions

Conceptualization, D.P., M.P. and I.T.; Methodology, D.P., R.P., P.J., S.I., H.K., T.B., and S.D.; Formal Analysis, D.P., P.J., S.T., E.C., S.I., K.J.S. and T.B.; Investigation, D.P., R.P., P.J., S.T., E.C., V.S., S.I., S.M., L.Z., H.K., N.C., K.J.S., J.Z., J.V., F.A., and S.M.; Resources, E.G., M.T, D.A., O.L., L.-M.P., S.D., J.U.-S., P.M.S., M.P., and I.T.; Writing – Original Draft, D.P., M.P., and I.T.; Writing – Review & Editing, all authors; Supervision, M.P., and I.T.; Project Administration, M.P., and I.T.; Funding Acquisition, D.P., M.P., and I.T.

Competing Interests

The authors declare no competing interests

Supplementary Tables

The online version contains supplementary tables.

Supplementary Table 1: List of Antibodies

Supplementary Table 2: Primer sequences used for RT-qPCR

Supplementary Table 3: Primer sequences used for ChIP-qPCR

Supplementary Table 4: gRNA sequences used for generation of ETFDH KO cell lines

Supplementary Table 5: Primer sequences used for sequencing

Material & Correspondence

Further information and requests for reagents may be directed upon reasonable request by the lead contact, Ivan Topisirovic (ivan.topisirovic@mcgill.ca).

References

1 Banerjee, R., Purhonen, J. & Kallijarvi, J. The mitochondrial coenzyme Q junction and complex III: biochemistry and pathophysiology. *FEBS J* **289**, 6936-6958 (2022). https://doi.org:10.1111/febs.16164

2 Mereis, M. *et al.* Disorders of flavin adenine dinucleotide metabolism: MADD and related deficiencies. *Int J Biochem Cell Biol* **132**, 105899 (2021). https://doi.org:10.1016/j.biocel.2020.105899

3 Ghisla, S. & Thorpe, C. Acyl-CoA dehydrogenases. A mechanistic overview. *Eur J Biochem* **271**, 494-508 (2004). https://doi.org:10.1046/j.1432-1033.2003.03946.x

4 Zhang, Y. *et al.* An acyl-CoA dehydrogenase microplate activity assay using recombinant porcine electron transfer flavoprotein. *Anal Biochem* **581**, 113332 (2019). https://doi.org:10.1016/j.ab.2019.06.003

5 El-Gharbawy, A. & Vockley, J. Inborn Errors of Metabolism with Myopathy: Defects of Fatty Acid Oxidation and the Carnitine Shuttle System. *Pediatr Clin North Am* **65**, 317-335 (2018). https://doi.org:10.1016/j.pcl.2017.11.006

6 Olsen, R. K. *et al.* ETFDH mutations as a major cause of riboflavin-responsive multiple acyl-CoA dehydrogenation deficiency. *Brain* **130**, 2045-2054 (2007). https://doi.org:10.1093/brain/awm135

7 Missaglia, S., Tavian, D. & Angelini, C. ETF dehydrogenase advances in molecular genetics and impact on treatment. *Crit Rev Biochem Mol Biol* **56**, 360-372 (2021). https://doi.org:10.1080/10409238.2021.1908952

8 Herrero Martin, J. C. *et al.* An ETFDH-driven metabolon supports OXPHOS efficiency in skeletal muscle by regulating coenzyme Q homeostasis. *Nat Metab* **6**, 209-225 (2024). https://doi.org:10.1038/s42255-023-00956-y

9 Bertomeu, T. *et al.* A High-Resolution Genome-Wide CRISPR/Cas9 Viability Screen Reveals Structural Features and Contextual Diversity of the Human Cell-Essential Proteome. *Mol Cell Biol* **38** (2018). https://doi.org:10.1128/MCB.00302-17

10 Tsherniak, A. *et al.* Defining a Cancer Dependency Map. *Cell* **170**, 564-576 e516 (2017). https://doi.org:10.1016/j.cell.2017.06.010

11 Ursini-Siegel, J. *et al.* ShcA signalling is essential for tumour progression in mouse models of human breast cancer. *EMBO J* **27**, 910-920 (2008). https://doi.org:10.1038/emboj.2008.22

12 Borowicz, S. *et al.* The soft agar colony formation assay. *J Vis Exp*, e51998 (2014). https://doi.org:10.3791/51998

13 DeBerardinis, R. J. & Cheng, T. Q's next: the diverse functions of glutamine in metabolism, cell biology and cancer. *Oncogene* **29**, 313-324 (2010). https://doi.org:10.1038/onc.2009.358

14 Saxton, R. A. & Sabatini, D. M. mTOR Signaling in Growth, Metabolism, and Disease. *Cell* **168**, 960-976 (2017). https://doi.org:10.1016/j.cell.2017.02.004

15 Thoreen, C. C. *et al.* An ATP-competitive mammalian target of rapamycin inhibitor reveals rapamycin-resistant functions of mTORC1. *J Biol Chem* **284**, 8023-8032 (2009). https://doi.org:10.1074/jbc.M900301200

16 Lee, B. J. *et al.* Selective inhibitors of mTORC1 activate 4EBP1 and suppress tumor growth. *Nat Chem Biol* **17**, 1065-1074 (2021). https://doi.org:10.1038/s41589-021-00813-7

17 Harding, H. P. *et al.* Regulated translation initiation controls stress-induced gene expression in mammalian cells. *Mol Cell* **6**, 1099-1108 (2000). https://doi.org:10.1016/s1097-2765(00)00108-8

18 Dowling, R. J. *et al.* mTORC1-mediated cell proliferation, but not cell growth, controlled by the 4E-BPs. *Science* **328**, 1172-1176 (2010). https://doi.org:10.1126/science.1187532

19 Gingras, A. C. *et al.* Regulation of 4E-BP1 phosphorylation: a novel two-step mechanism. *Genes Dev* **13**, 1422-1437 (1999). https://doi.org:10.1101/gad.13.11.1422

20 Hulea, L. *et al.* Translational and HIF-1alpha-Dependent Metabolic Reprogramming Underpin Metabolic Plasticity and Responses to Kinase Inhibitors and Biguanides. *Cell Metab* **28**, 817-832 e818 (2018). https://doi.org:10.1016/j.cmet.2018.09.001

21 Morita, M. *et al.* mTORC1 controls mitochondrial activity and biogenesis through 4E-BP-dependent translational regulation. *Cell Metab* **18**, 698-711 (2013). https://doi.org:10.1016/j.cmet.2013.10.001

22 Morita, M. *et al.* mTOR coordinates protein synthesis, mitochondrial activity and proliferation. *Cell Cycle* **14**, 473-480 (2015). https://doi.org:10.4161/15384101.2014.991572

23 Yamaguchi, S. *et al.* ATF4-mediated induction of 4E-BP1 contributes to pancreatic beta cell survival under endoplasmic reticulum stress. *Cell Metab* **7**, 269-276 (2008). https://doi.org:10.1016/j.cmet.2008.01.008

24 Wang, J. *et al.* Snail determines the therapeutic response to mTOR kinase inhibitors by transcriptional repression of 4E-BP1. *Nat Commun* **8**, 2207 (2017). https://doi.org:10.1038/s41467-017-02243-3

25 Totten, S. P. *et al.* STAT1 potentiates oxidative stress revealing a targetable vulnerability that increases phenformin efficacy in breast cancer. *Nat Commun* **12**, 3299 (2021). https://doi.org:10.1038/s41467-021-23396-2

26 Hayes, J. D., Dinkova-Kostova, A. T. & Tew, K. D. Oxidative Stress in Cancer. *Cancer Cell* **38**, 167-197 (2020). https://doi.org:10.1016/j.ccell.2020.06.001

27 Nakayamada, S. *et al.* Type I IFN induces binding of STAT1 to Bcl6: divergent roles of STAT family transcription factors in the T follicular helper cell genetic program. *J Immunol* **192**, 2156-2166 (2014). https://doi.org:10.4049/jimmunol.1300675

28 Liu, Y. *et al.* The oncoprotein BCL6 enables solid tumor cells to evade genotoxic stress. *Elife* **11** (2022). https://doi.org:10.7554/eLife.69255

29 Madapura, H. S. *et al.* Interferon gamma is a STAT1-dependent direct inducer of BCL6 expression in imatinib-treated chronic myeloid leukemia cells. *Oncogene* **36**, 4619-4628 (2017). https://doi.org:10.1038/onc.2017.85

30 Ramachandran, K. *et al.* Transcriptional programming of translation by BCL6 controls skeletal muscle proteostasis. *Nat Metab* **6**, 304-322 (2024). https://doi.org:10.1038/s42255-024-00983-3

31 Yi, W. *et al.* The mTORC1-4E-BP-eIF4E axis controls de novo Bcl6 protein synthesis in T cells and systemic autoimmunity. *Nat Commun* **8**, 254 (2017). https://doi.org:10.1038/s41467-017-00348-3

32 Xu, L. *et al.* The Kinase mTORC1 Promotes the Generation and Suppressive Function of Follicular Regulatory T Cells. *Immunity* **47**, 538-551 e535 (2017). https://doi.org:10.1016/j.immuni.2017.08.011

33 Raybuck, A. L. *et al.* B Cell-Intrinsic mTORC1 Promotes Germinal Center-Defining Transcription Factor Gene Expression, Somatic Hypermutation, and Memory B Cell Generation in Humoral Immunity. *J Immunol* **200**, 2627-2639 (2018). https://doi.org:10.4049/jimmunol.1701321

34 Consortium, I. T. P.-C. A. o. W. G. Pan-cancer analysis of whole genomes. *Nature* **578**, 82-93 (2020). https://doi.org:10.1038/s41586-020-1969-6

35 Powell, G., Pavlovic Djuranovic, S. & Djuranovic, S. Gene dosage effects of poly(A) track-engineered hypomorphs. *Mol Ther Nucleic Acids* **26**, 865-878 (2021). https://doi.org:10.1016/j.omtn.2021.10.005

36 Arthur, L. *et al.* Translational control by lysine-encoding A-rich sequences. *Sci Adv* **1** (2015). https://doi.org:10.1126/sciadv.1500154

37 Jumper, J. *et al.* Highly accurate protein structure prediction with AlphaFold. *Nature* **596**, 583-589 (2021). https://doi.org:10.1038/s41586-021-03819-2

38 Varadi, M. *et al.* AlphaFold Protein Structure Database: massively expanding the structural coverage of protein-sequence space with high-accuracy models. *Nucleic Acids Res* **50**, D439-D444 (2022). https://doi.org:10.1093/nar/gkab1061

39 Jones, P. A. & Baylin, S. B. The fundamental role of epigenetic events in cancer. *Nat Rev Genet* **3**, 415-428 (2002). https://doi.org:10.1038/nrg816

40 Nilsson, R. *et al.* Metabolic enzyme expression highlights a key role for MTHFD2 and the mitochondrial folate pathway in cancer. *Nat Commun* **5**, 3128 (2014). https://doi.org:10.1038/ncomms4128

41 Smith, H. W. *et al.* An ErbB2/c-Src axis links bioenergetics with PRC2 translation to drive epigenetic reprogramming and mammary tumorigenesis. *Nat Commun* **10**, 2901 (2019). https://doi.org:10.1038/s41467-019-10681-4

42 Harachi, M. *et al.* Dual Regulation of Histone Methylation by mTOR Complexes Controls Glioblastoma Tumor Cell Growth via EZH2 and SAM. *Mol Cancer Res* **18**, 1142-1152 (2020). https://doi.org:10.1158/1541-7786.MCR-20-0024

43 Chen, M. *et al.* The activation of mTOR signalling modulates DNA methylation by enhancing DNMT1 translation in hepatocellular carcinoma. *J Transl Med* **21**, 276 (2023). https://doi.org:10.1186/s12967-023-04103-9

44 Kim, H. *et al.* MTOR modulation induces selective perturbations in histone methylation which influence the anti-proliferative effects of mTOR inhibitors. *iScience* **27**, 109188 (2024). https://doi.org:10.1016/j.isci.2024.109188

45 Petroulakis, E. *et al.* p53-dependent translational control of senescence and transformation via 4E-BPs. *Cancer Cell* **16**, 439-446 (2009). https://doi.org:10.1016/j.ccr.2009.09.025

46 Hsieh, A. C. *et al.* Genetic dissection of the oncogenic mTOR pathway reveals druggable addiction to translational control via 4EBP-eIF4E. *Cancer Cell* **17**, 249-261 (2010). https://doi.org:10.1016/j.ccr.2010.01.021

47 Polunovsky, V. A. *et al.* Translational control of the antiapoptotic function of Ras. *J Biol Chem* **275**, 24776-24780 (2000). https://doi.org:10.1074/jbc.M001938200

48 Lynch, M., Fitzgerald, C., Johnston, K. A., Wang, S. & Schmidt, E. V. Activated eIF4E-binding protein slows G1 progression and blocks transformation by c-myc without inhibiting cell growth. *J Biol Chem* **279**, 3327-3339 (2004). https://doi.org:10.1074/jbc.M310872200

49 Avdulov, S. *et al.* Activation of translation complex eIF4F is essential for the genesis and maintenance of the malignant phenotype in human mammary epithelial cells. *Cancer Cell* **5**, 553-563 (2004). https://doi.org:10.1016/j.ccr.2004.05.024

50 Rousseau, D., Gingras, A. C., Pause, A. & Sonenberg, N. The eIF4E-binding proteins 1 and 2 are negative regulators of cell growth. *Oncogene* **13**, 2415-2420 (1996).

51 Musa, J. *et al.* Eukaryotic initiation factor 4E-binding protein 1 (4E-BP1): a master regulator of mRNA translation involved in tumorigenesis. *Oncogene* **35**, 4675-4688 (2016). https://doi.org:10.1038/onc.2015.515

52 Jewer, M. *et al.* Translational control of breast cancer plasticity. *Nat Commun* **11**, 2498 (2020). https://doi.org:10.1038/s41467-020-16352-z

53 Teleman, A. A., Chen, Y. W. & Cohen, S. M. 4E-BP functions as a metabolic brake used under stress conditions but not during normal growth. *Genes Dev* **19**, 1844-1848 (2005). https://doi.org:10.1101/gad.341505

54 Levy, T. *et al.* mTORC1 regulates cell survival under glucose starvation through 4EBP1/2-mediated translational reprogramming of fatty acid metabolism. *Nat Commun* **15**, 4083 (2024). https://doi.org:10.1038/s41467-024-48386-y

55 Tabaries, S. *et al.* Claudin-2 promotes colorectal cancer liver metastasis and is a biomarker of the replacement type growth pattern. *Commun Biol* **4**, 657 (2021). https://doi.org:10.1038/s42003-021-02189-9

56 Igelmann, S. *et al.* A hydride transfer complex reprograms NAD metabolism and bypasses senescence. *Mol Cell* **81**, 3848-3865 e3819 (2021). https://doi.org:10.1016/j.molcel.2021.08.028

57 Gandin, V. *et al.* Polysome fractionation and analysis of mammalian translatomes on a genome-wide scale. *J Vis Exp* (2014). https://doi.org:10.3791/51455

58 Papadopoli, D. *et al.* Perturbations of cancer cell metabolism by the antidiabetic drug canagliflozin. *Neoplasia* **23**, 391-399 (2021). https://doi.org:10.1016/j.neo.2021.02.003

59 McGuirk, S. *et al.* PGC-1alpha supports glutamine metabolism in breast cancer. *Cancer Metab* **1**, 22 (2013). https://doi.org:10.1186/2049-3002-1-22

60 Mookerjee, S. A., Gerencser, A. A., Nicholls, D. G. & Brand, M. D. Quantifying intracellular rates of glycolytic and oxidative ATP production and consumption using extracellular flux measurements. *J Biol Chem* **292**, 7189-7207 (2017). https://doi.org:10.1074/jbc.M116.774471

61 Topisirovic, I. *et al.* Stability of eukaryotic translation initiation factor 4E mRNA is regulated by HuR, and this activity is dysregulated in cancer. *Mol Cell Biol* **29**, 1152-1162 (2009). https://doi.org:10.1128/MCB.01532-08

62 Labun, K. *et al.* CHOPCHOP v3: expanding the CRISPR web toolbox beyond genome editing. *Nucleic Acids Res* **47**, W171-W174 (2019). https://doi.org:10.1093/nar/gkz365

63 Sanjana, N. E., Shalem, O. & Zhang, F. Improved vectors and genome-wide libraries for CRISPR screening. *Nat Methods* **11**, 783-784 (2014). https://doi.org:10.1038/nmeth.3047

64 Shalem, O. *et al.* Genome-scale CRISPR-Cas9 knockout screening in human cells. *Science* **343**, 84-87 (2014). https://doi.org:10.1126/science.1247005

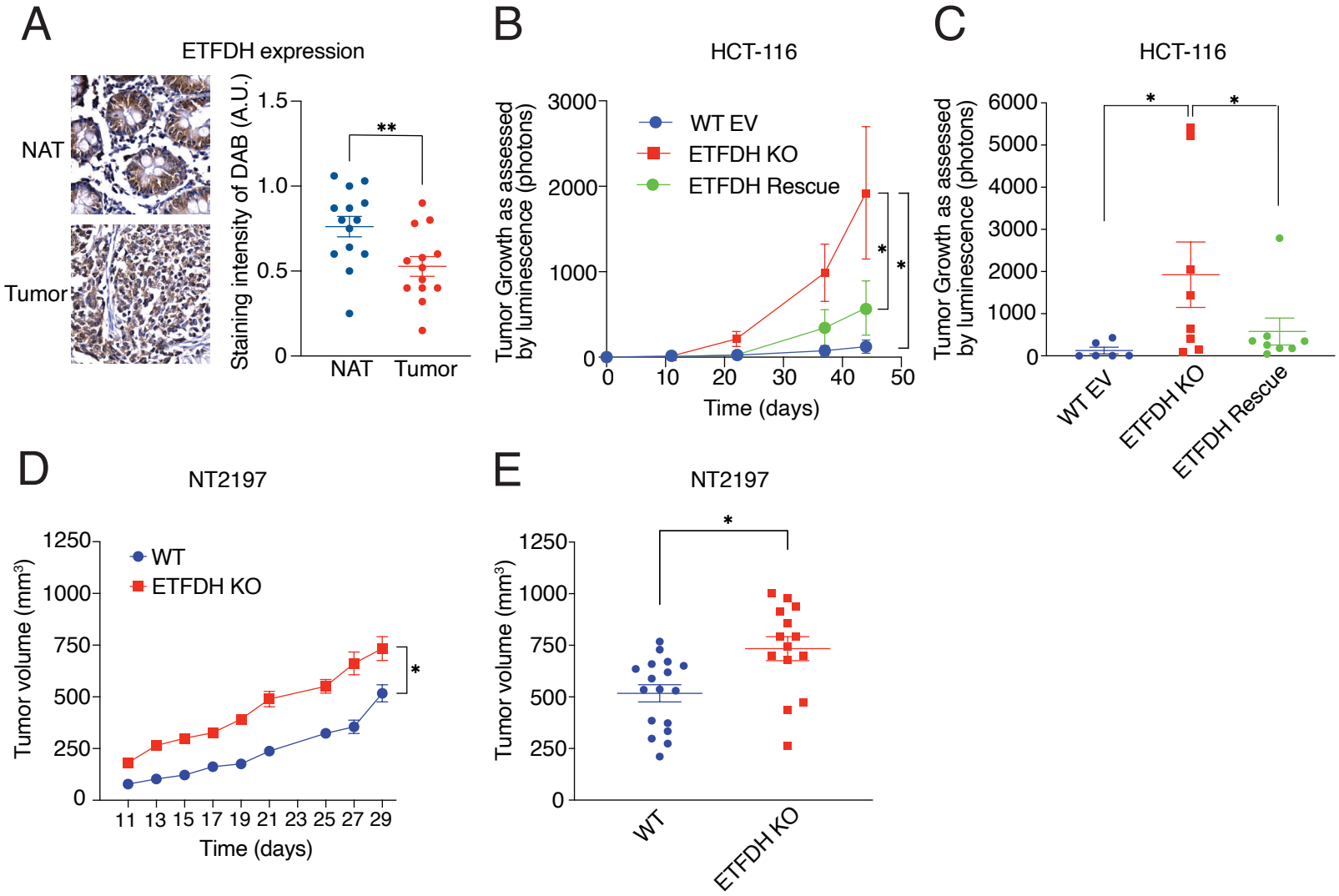
A
ETFDH expression
NAT
Tumor
Staining intensity of DAB (A.U.)
1.5
1.0
0.5
0
**
NAT
Tumor
B
HCT-116
Tumor Growth as assessed by luminescence (photons)
3000
2000
1000
0
WT EV
ETFDH KO
ETFDH Rescue
*
*
0
10
20
30
40
50
Time (days)
C
HCT-116
Tumor Growth as assessed by luminescence (photons)
6000
5000
4000
3000
2000
1000
0
*
*
WT EV
ETFDH KO
ETFDH Rescue
D
NT2197
Tumor volume (mm3)
1250
1000
750
500
250
0
WT
ETFDH KO
*
11 13 15 17 19 21 23 25 27 29
Time (days)
E
NT2197
Tumor volume (mm3)
1250
1000
750
500
250
0
*
WT
ETFDH KO

Fig.1

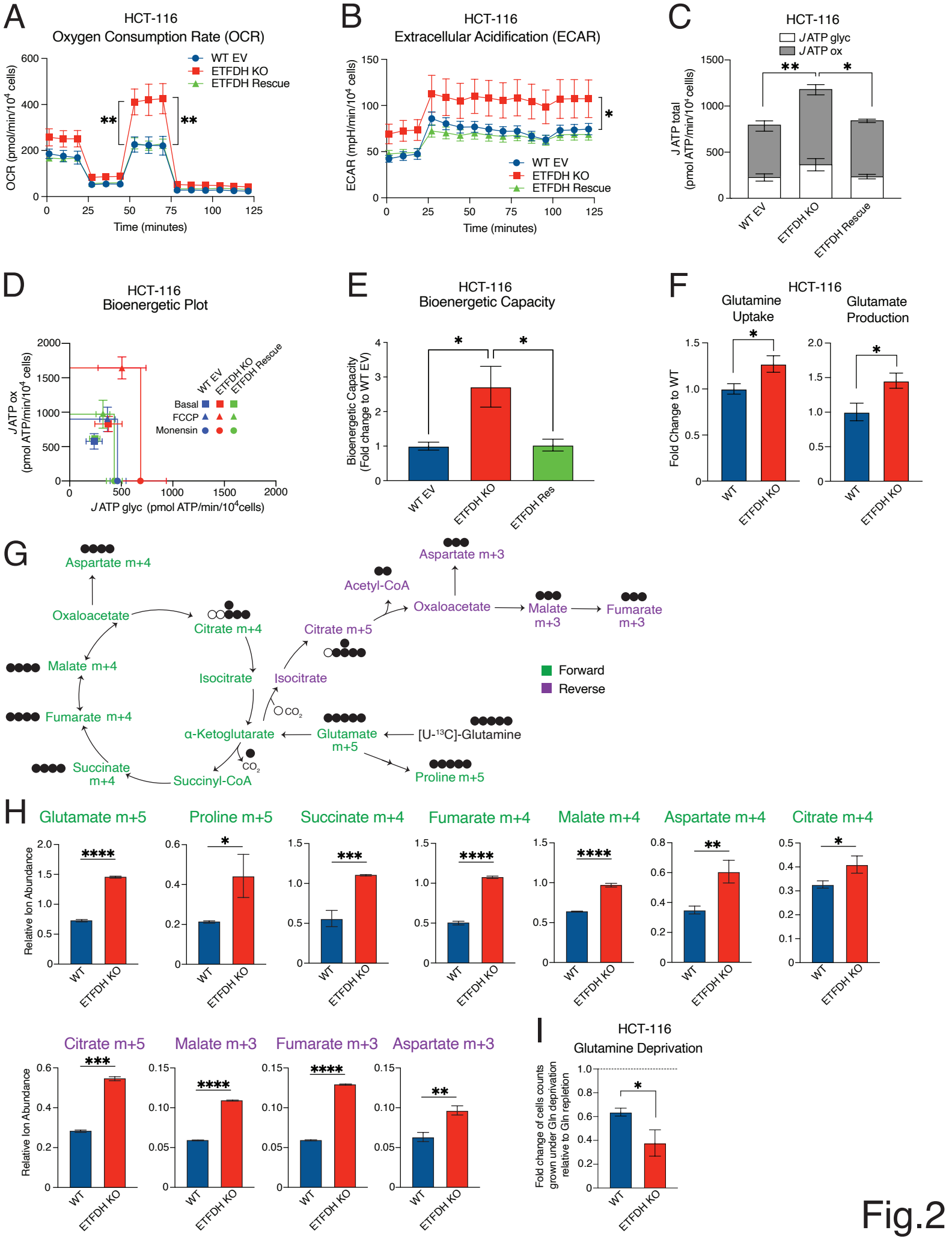
A
HCT-116
Oxygen Consumption Rate (OCR)
WT EV
ETFDH KO
ETFDH Rescue
OCR (pmol/min/10^4 cells)
Time (minutes)
B
HCT-116
Extracellular Acidification (ECAR)
ECAR (mpH/min/10^4 cells)
Time (minutes)
C
HCT-116
J ATP glyc
J ATP ox
J ATP total (pmol ATP/min/10^4 cells)
WT EV
ETFDH KO
ETFDH Rescue
D
HCT-116
Bioenergetic Plot
J ATP ox (pmol ATP/min/10^4 cells)
J ATP glyc (pmol ATP/min/10^4cells)
Basal
FCCP
Monensin
E
HCT-116
Bioenergetic Capacity
Bioenergetic Capacity (Fold change to WT EV)
WT EV
ETFDH KO
ETFDH Res
F
HCT-116
Glutamine Uptake
Glutamate Production
Fold Change to WT
WT
ETFDH KO
G
Aspartate m+4
Oxaloacetate
Citrate m+4
Malate m+4
Isocitrate
Fumarate m+4
α-Ketoglutarate
Succinate m+4
Succinyl-CoA
Citrate m+5
Isocitrate
Acetyl-CoA
Aspartate m+3
Oxaloacetate
Malate m+3
Fumarate m+3
Glutamate m+5
[U-13C]-Glutamine
Proline m+5
Forward
Reverse
H
Glutamate m+5
Proline m+5
Succinate m+4
Fumarate m+4
Malate m+4
Aspartate m+4
Citrate m+4
Citrate m+5
Malate m+3
Fumarate m+3
Aspartate m+3
Relative Ion Abundance
WT
ETFDH KO
I
HCT-116
Glutamine Deprivation
Fold change of cells counts grown under Gln deprivation relative to Gln repletion
WT
ETFDH KO

Fig.2

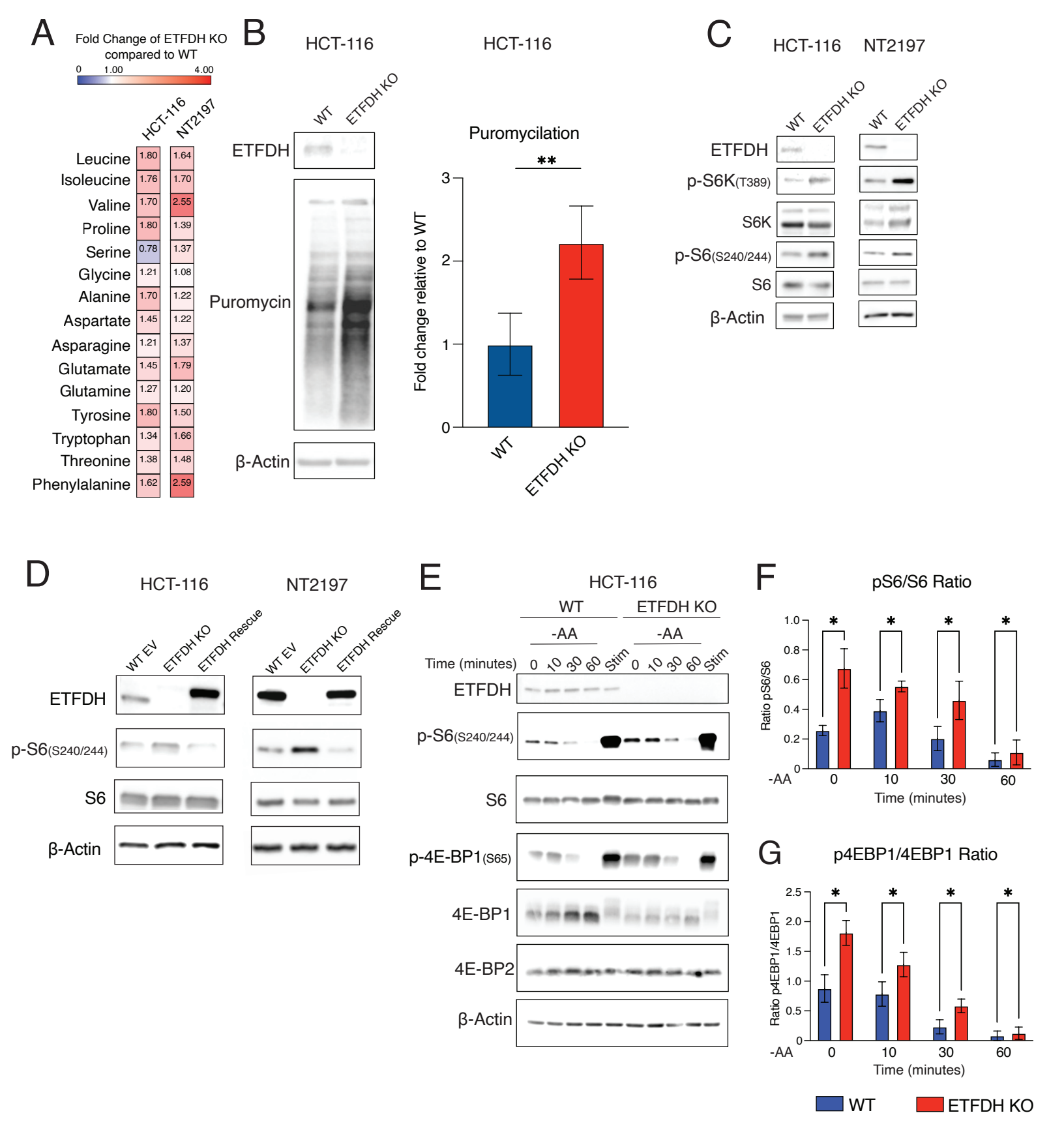
A
Fold Change of ETFDH KO compared to WT
0
1.00
4.00
HCT-116
NT2197
Leucine 1.80 1.64
Isoleucine 1.76 1.70
Valine 1.70 2.55
Proline 1.80 1.39
Serine 0.78 1.37
Glycine 1.21 1.08
Alanine 1.70 1.22
Aspartate 1.45 1.22
Asparagine 1.21 1.37
Glutamate 1.45 1.79
Glutamine 1.27 1.20
Tyrosine 1.80 1.50
Tryptophan 1.34 1.66
Threonine 1.38 1.48
Phenylalanine 1.62 2.59
B
HCT-116
WT
ETFDH KO
ETFDH
Puromycin
β-Actin
HCT-116
Puromycilation
**
Fold change relative to WT
0
1
2
3
WT
ETFDH KO
C
HCT-116
NT2197
WT
ETFDH KO
WT
ETFDH KO
ETFDH
p-S6K(T389)
S6K
p-S6(S240/244)
S6
β-Actin
D
HCT-116
NT2197
WT EV
ETFDH KO
ETFDH Rescue
WT EV
ETFDH KO
ETFDH Rescue
ETFDH
p-S6(S240/244)
S6
β-Actin
E
HCT-116
WT
ETFDH KO
-AA
-AA
Time (minutes)
0
10
30
60
Stim
0
10
30
60
Stim
ETFDH
p-S6(S240/244)
S6
p-4E-BP1(S65)
4E-BP1
4E-BP2
β-Actin
F
pS6/S6 Ratio
Ratio pS6/S6
0
0.2
0.4
0.6
0.8
1.0
*
*
*
*
-AA
0
10
30
60
Time (minutes)
G
p4EBP1/4EBP1 Ratio
Ratio p4EBP1/4EBP1
0
0.5
1.0
1.5
2.0
2.5
*
*
*
*
-AA
0
10
30
60
Time (minutes)
WT
ETFDH KO

Fig.3

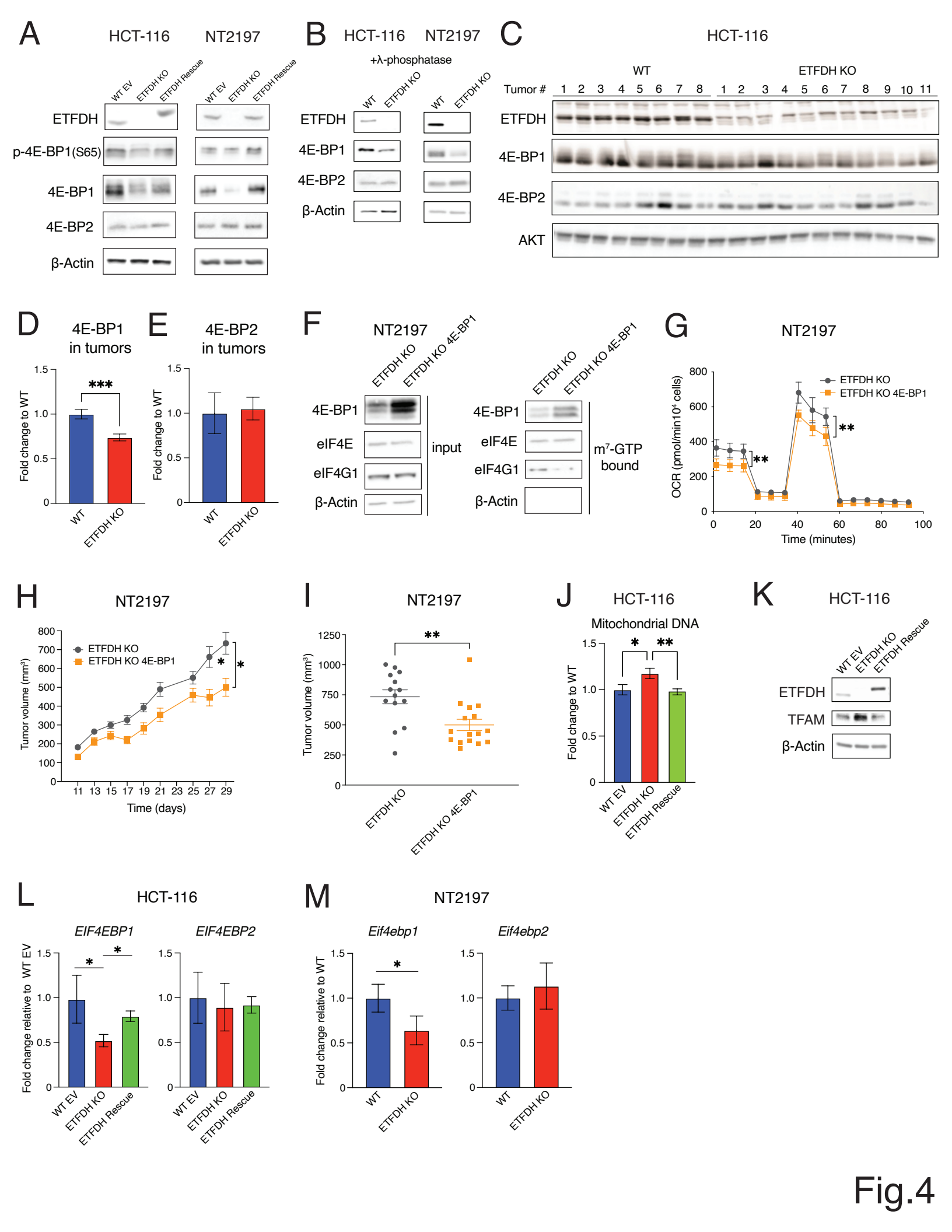
A
HCT-116
NT2197
WT EV
ETFDH KO
ETFDH Rescue
ETFDH
p-4E-BP1(S65)
4E-BP1
4E-BP2
β-Actin
B
HCT-116
NT2197
+λ-phosphatase
WT
ETFDH KO
ETFDH
4E-BP1
4E-BP2
β-Actin
C
HCT-116
WT
ETFDH KO
Tumor #
1 2 3 4 5 6 7 8 1 2 3 4 5 6 7 8 9 10 11
ETFDH
4E-BP1
4E-BP2
AKT
D
4E-BP1
in tumors
Fold change to WT
***
WT
ETFDH KO
E
4E-BP2
in tumors
Fold change to WT
WT
ETFDH KO
F
NT2197
ETFDH KO
ETFDH KO 4E-BP1
4E-BP1
eIF4E
eIF4G1
β-Actin
input
m7-GTP
bound
G
NT2197
ETFDH KO
ETFDH KO 4E-BP1
OCR (pmol/min10⁴ cells)
Time (minutes)
**
H
NT2197
ETFDH KO
ETFDH KO 4E-BP1
Tumor volume (mm³)
Time (days)
*
I
NT2197
Tumor volume (mm³)
**
ETFDH KO
ETFDH KO 4E-BP1
J
HCT-116
Mitochondrial DNA
Fold change to WT
WT EV
ETFDH KO
ETFDH Rescue
K
HCT-116
WT EV
ETFDH KO
ETFDH Rescue
ETFDH
TFAM
β-Actin
L
HCT-116
EIF4EBP1
EIF4EBP2
Fold change relative to WT EV
WT EV
ETFDH KO
ETFDH Rescue
M
NT2197
Eif4ebp1
Eif4ebp2
Fold change relative to WT
WT
ETFDH KO

Fig.4

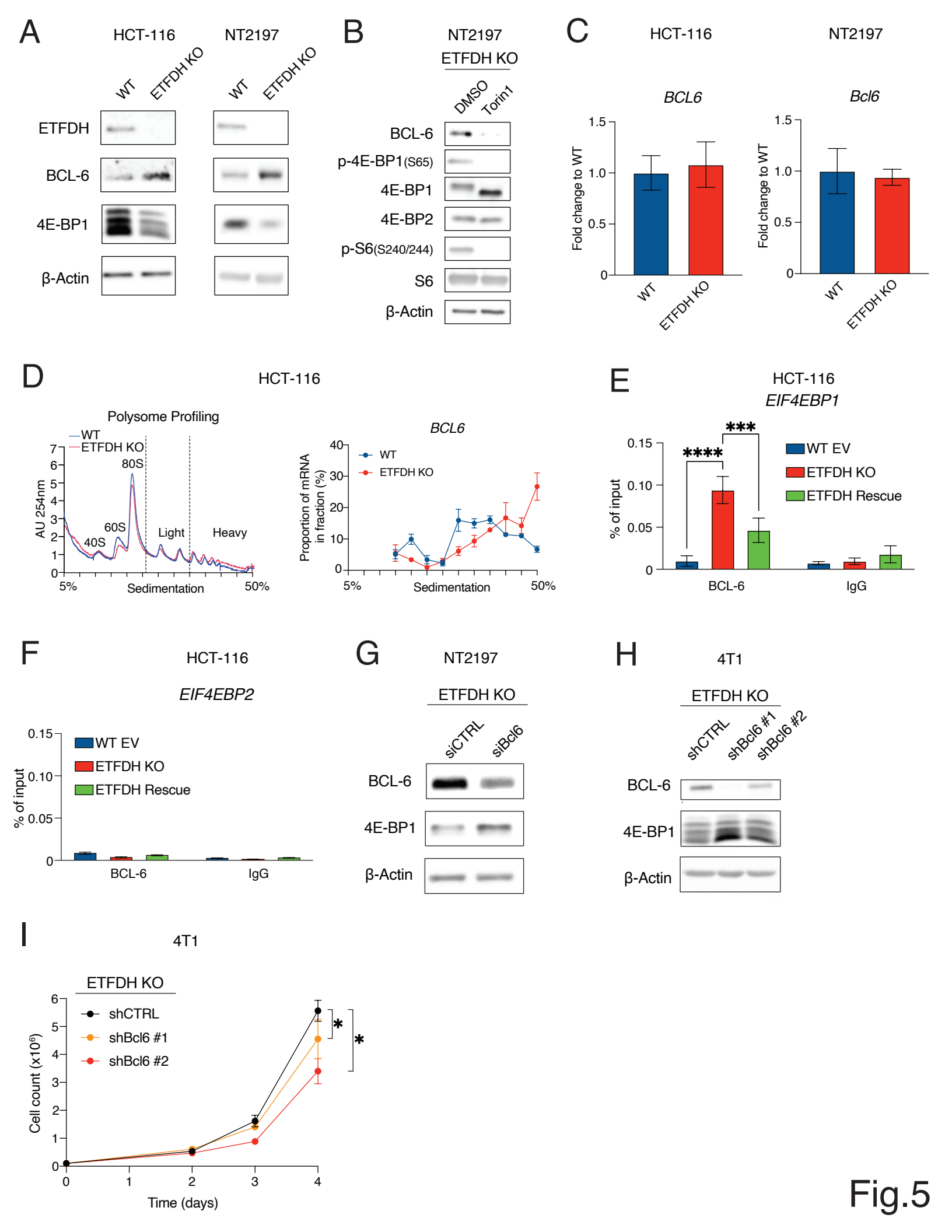
A
HCT-116
NT2197
WT
ETFDH KO
WT
ETFDH KO
ETFDH
BCL-6
4E-BP1
β-Actin
B
NT2197
ETFDH KO
DMSO
Torin1
BCL-6
p-4E-BP1(S65)
4E-BP1
4E-BP2
p-S6(S240/244)
S6
β-Actin
C
HCT-116
NT2197
BCL6
Bcl6
Fold change to WT
1.5
1.0
0.5
0
WT
ETFDH KO
D
HCT-116
Polysome Profiling
WT
ETFDH KO
AU 254nm
80S
60S
40S
Light
Heavy
5%
Sedimentation
50%
BCL6
Proportion of mRNA in fraction (%)
40
30
20
10
0
WT
ETFDH KO
5%
Sedimentation
50%
E
HCT-116
EIF4EBP1
% of input
0.15
0.10
0.05
0
****
***
WT EV
ETFDH KO
ETFDH Rescue
BCL-6
IgG
F
HCT-116
EIF4EBP2
% of input
0.15
0.10
0.05
0
WT EV
ETFDH KO
ETFDH Rescue
BCL-6
IgG
G
NT2197
ETFDH KO
siCTRL
siBcl6
BCL-6
4E-BP1
β-Actin
H
4T1
ETFDH KO
shCTRL
shBcl6 #1
shBcl6 #2
BCL-6
4E-BP1
β-Actin
I
4T1
ETFDH KO
shCTRL
shBcl6 #1
shBcl6 #2
Cell count (x10⁶)
6
5
4
3
2
1
0
*
*
0
1
2
3
4
Time (days)

Fig.5

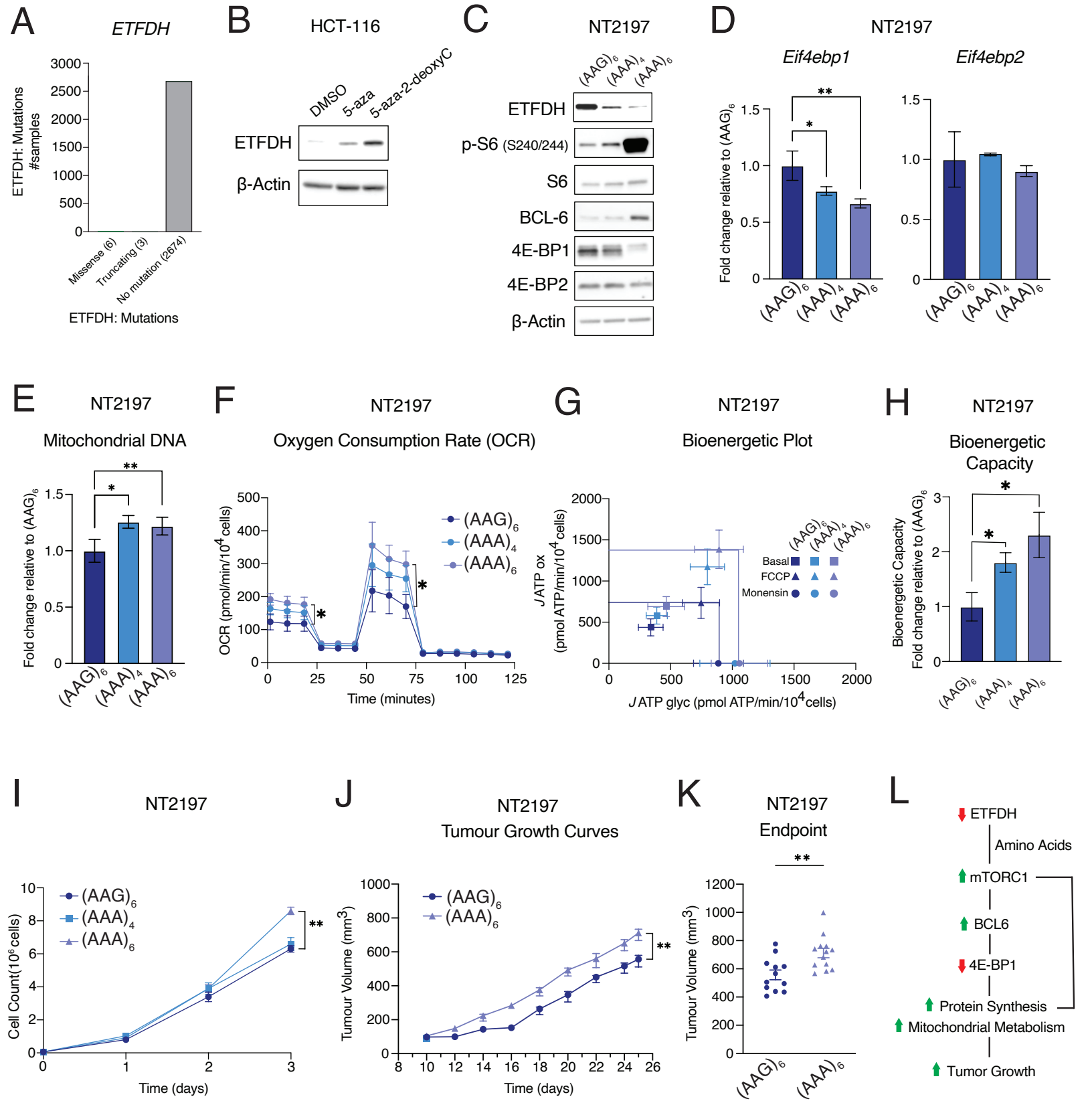
A
ETFDH
ETFDH: Mutations #samples
3000
2500
2000
1500
1000
500
0
Missense (6)
Truncating (3)
No mutation (2674)
ETFDH: Mutations
B
HCT-116
DMSO
5-aza
5-aza-2-deoxyC
ETFDH
β-Actin
C
NT2197
(AAG)6
(AAA)4
(AAA)6
ETFDH
p-S6 (S240/244)
S6
BCL-6
4E-BP1
4E-BP2
β-Actin
D
NT2197
Eif4ebp1
Eif4ebp2
Fold change relative to (AAG)6
E
NT2197
Mitochondrial DNA
Fold change relative to (AAG)6
F
NT2197
Oxygen Consumption Rate (OCR)
OCR (pmol/min/10^4 cells)
Time (minutes)
G
NT2197
Bioenergetic Plot
J ATP ox (pmol ATP/min/10^4 cells)
J ATP glyc (pmol ATP/min/10^4 cells)
Basal
FCCP
Monensin
H
NT2197
Bioenergetic Capacity
Bioenergetic Capacity
Fold change relative to (AAG)6
I
NT2197
Cell Count(10^6 cells)
Time (days)
J
NT2197
Tumour Growth Curves
Tumour Volume (mm^3)
Time (days)
K
NT2197
Endpoint
Tumour Volume (mm^3)
L
ETFDH
Amino Acids
mTORC1
BCL6
4E-BP1
Protein Synthesis
Mitochondrial Metabolism
Tumor Growth

Fig.6

Supplementary Figure 1

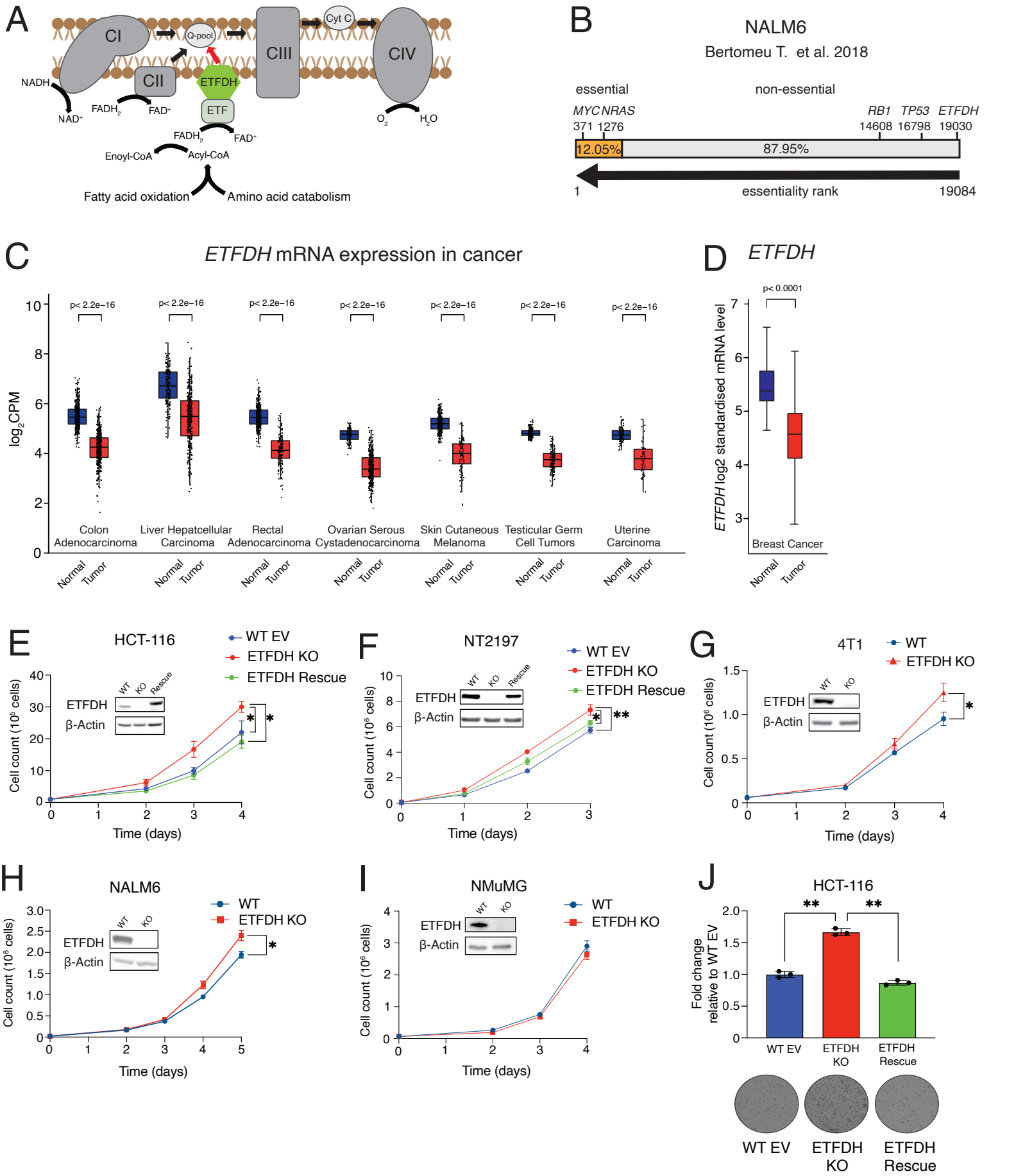

Supplementary Figure 2

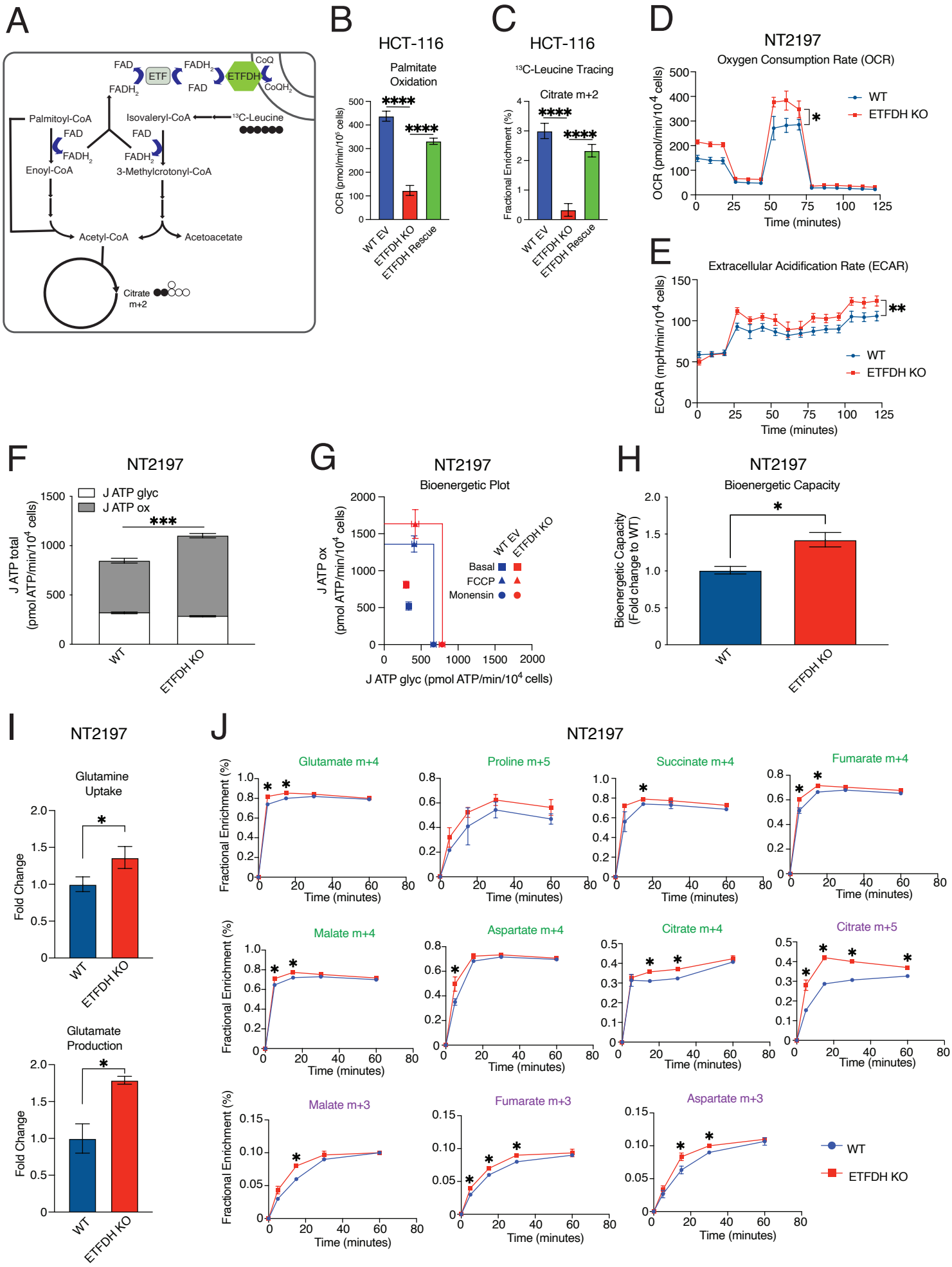

Supplementary Figure 3

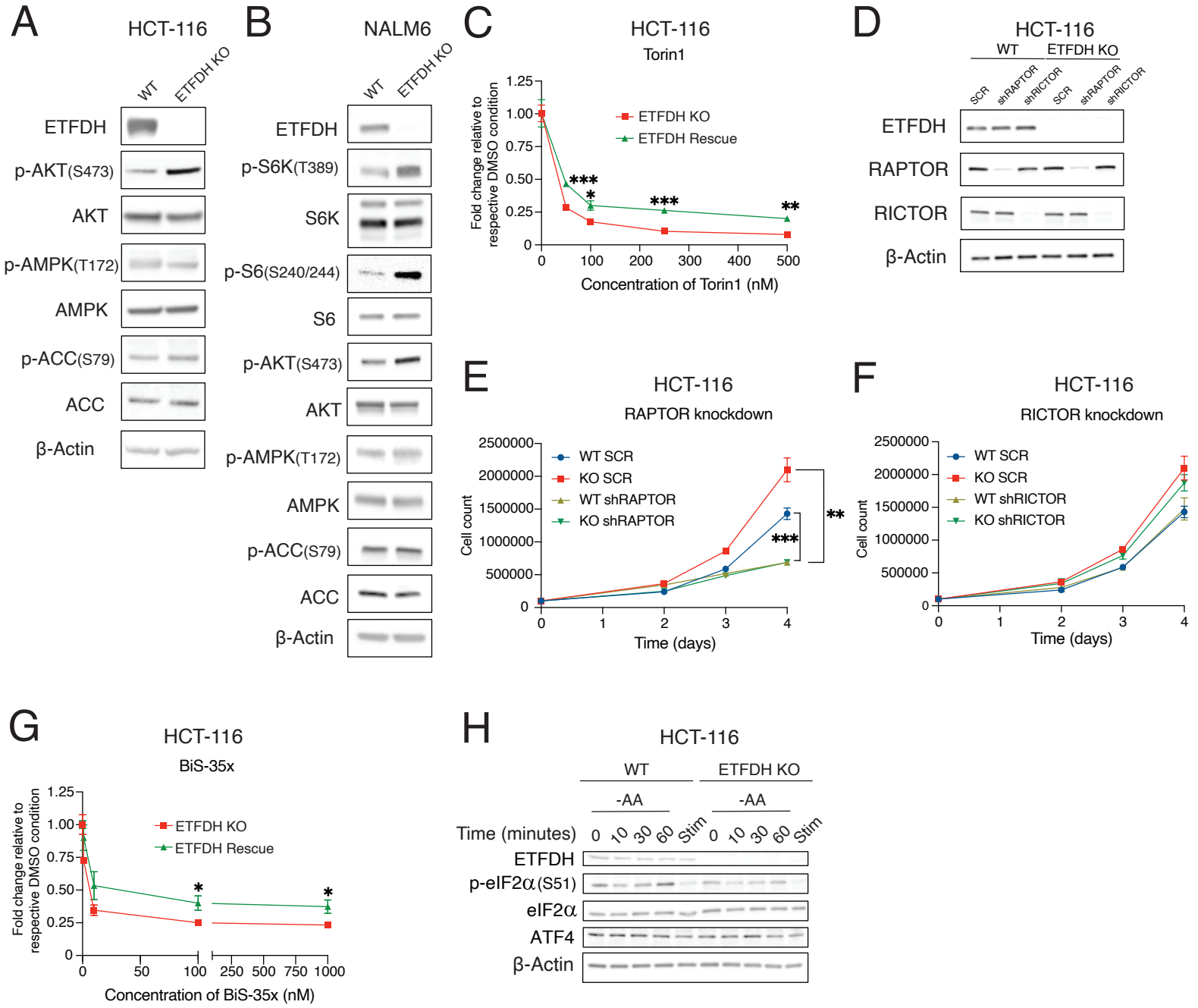

Supplementary Figure 4

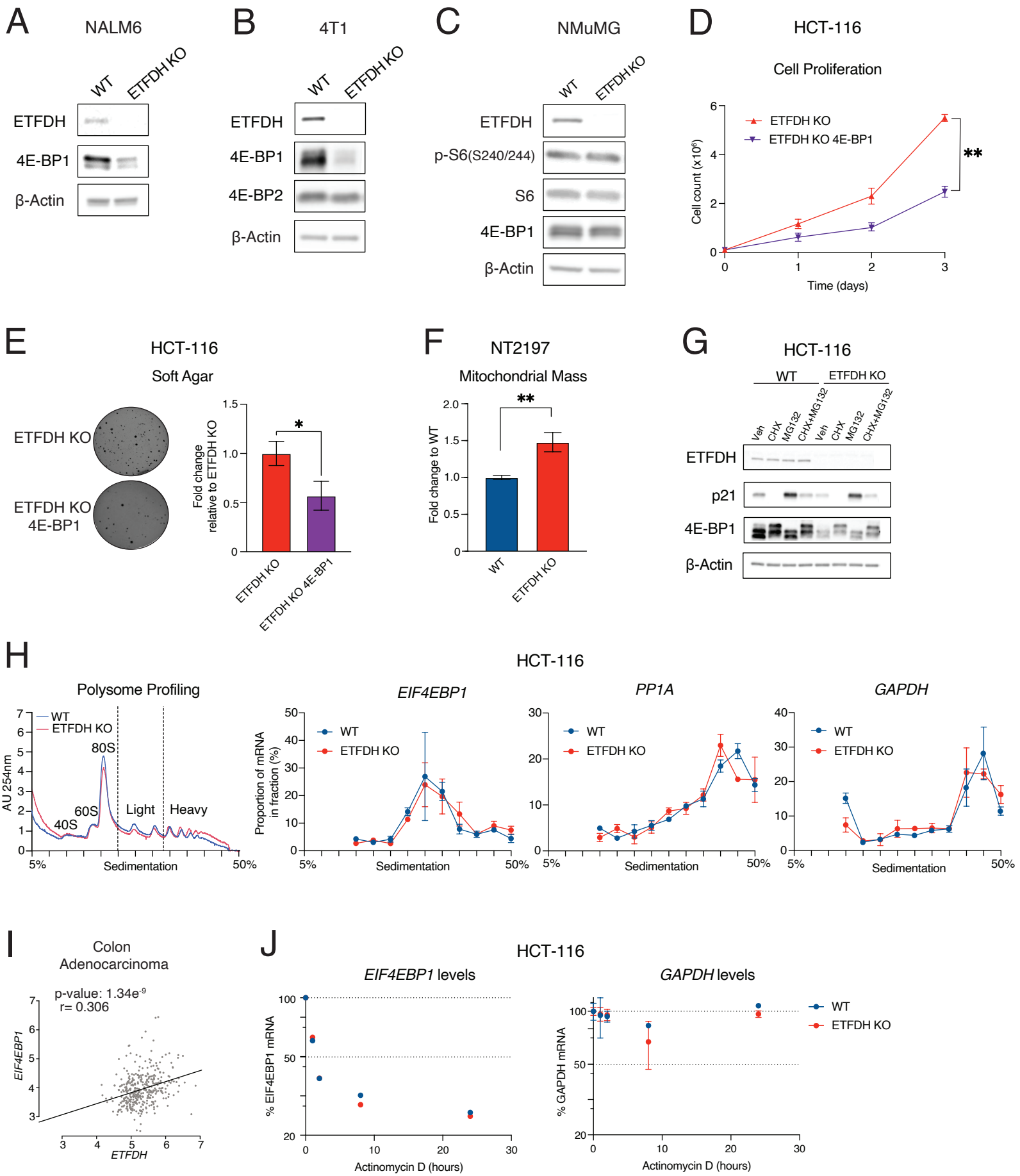

Supplementary Figure 5

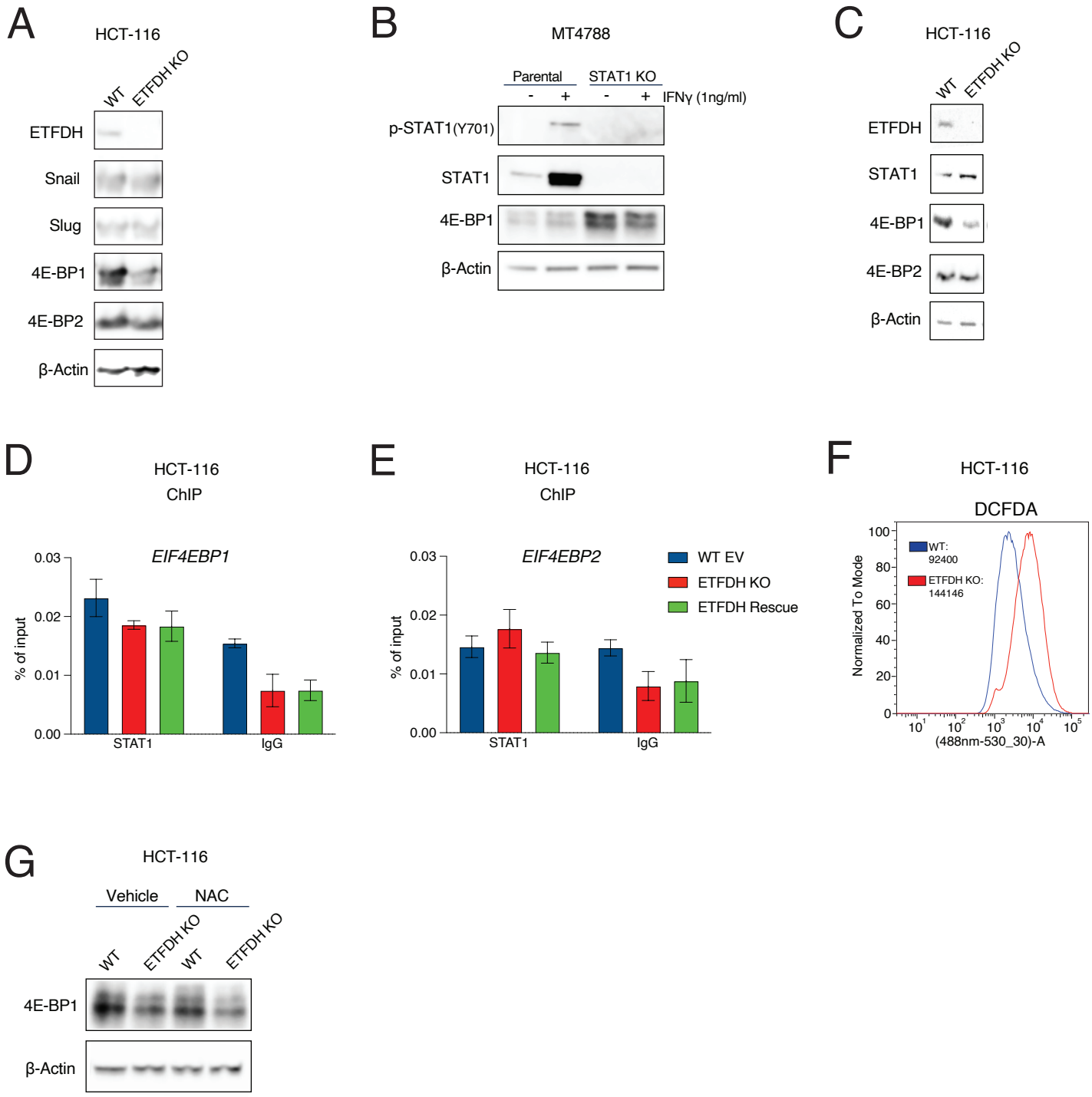

Supplementary Figure 6

A

```
                1                                                                                                                                                                                                                                                                                                                                                                                                                                                                                                                                                                                                                                                                                                                                                                                                                                                                                                                                                                                                                                                                                                                                                                                                                                                                                                                                                                                                                                                                                                                                                                                                                                                                                                                                                                                                                                                                                                                                                                                                                                                                                                                                                                                                                                                                                                                                                                                                                                                                                                                                                                                                                                                                                                                                                                                                                                                                                                                                                                                                                                                                                                                                                                                                                                                                                                                                                                                                                                                                                                                                                                                                                                                                                                                                                                                                                                                                                                                                                                                                                                                                                                                                                                                                                                                                                                                                                                                                                                                                                                                                                                                                                                                                                                                                                                                                                                                                                                                                                                                                                                                                                                                                                                                                                                                                                                                                                                                                                                                                                                                                                                                                                                                                                                                                                                                                                                                                                                                                                                                                                                                                                                                                                                                                                                                                                                                                                                                                                                                                                                                                                                                                                                                                                                                                                                                                                                                                                                                                                                                                                                                                                                                                                                                                                                                                                                                                                                                                                                                                                                                                                                                                                                                                                                                                                                                                                                                                                                                                                                                                                                                                                                                                                                                                                                                                                                                                                                                                                                                                                                                                                                                                                                
WT Etfdh   ATGTTGGTGCGACTAACCAAGCTGTCCTGCCCTGCGTATCACTGGTTTCATGCCTTAAAAATTAAGAAGTGCCTACCTCTGTGTGCTCCAAGATGTTCTTCAAACCTCTGCTGTA————————————————CCTCAGATTACCACTCACTACACTGTTCATCCCCGGGAGA....
(AAG)6     ATGTTGGTGCGACTAACCAAGCTGTCCTGCCCTGCGTATCACTGGTTTCATGCCTTAAAAATTAAGAAGTGCCTACCTCTGTGTGCTCCAAGATGTTCTTCAAACCTCTGCTGTAAAGAAGAAGAAGAAGAAGCCTCAGATTACCACTCACTACACTGTTCATCCCCGGGAGA....
(AAA)4     ATGTTGGTGCGACTAACCAAGCTGTCCTGCCCTGCGTATCACTGGTTTCATGCCTTAAAAATTAAGAAGTGCCTACCTCTGTGTGCTCCAAGATGTTCTTCAAACCTCTGCTGTAAAAAAAAAAAA————CCTCAGATTACCACTCACTACACTGTTCATCCCCGGGAGA....
(AAA)6     ATGTTGGTGCGACTAACCAAGCTGTCCTGCCCTGCGTATCACTGGTTTCATGCCTTAAAAATTAAGAAGTGCCTACCTCTGTGTGCTCCAAGATGTTCTTCAAACCTCTGCTGTAAAAAAAAAAAAAAAAAACCTCAGATTACCACTCACTACACTGTTCATCCCCGGGAGA....
```

B
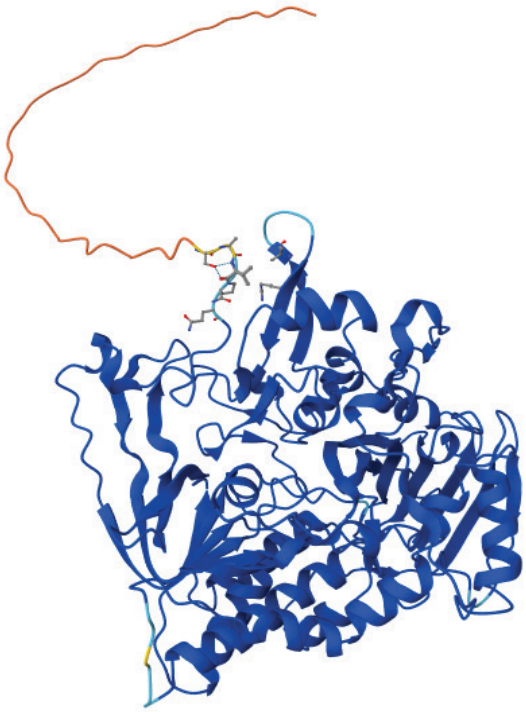
(AAG)6 / (AAA)6 Protein Structure